Ocean Modelling 132 (2018) 46–60

Contents lists available at ScienceDirect

Ocean Modelling

journal homepage: www.elsevier.com/locate/ocemod

Assimilation of coastal and open sea biogeochemical data to improve phytoplankton simulation in the Mediterranean Sea

Anna Teruzzi*[,a], Giorgio Bolzon[a], Stefano Salon[a], Paolo Lazzari[a], Cosimo Solidoro[a], Gianpiero Cossarini[a]

[a] Istituto Nazionale di Oceanografia e di Geofisica Sperimentale (OGS), Borgo Grotta Gigante 42/C, Sgonico (TS) 34010, Italy

ARTICLE INFO

Keywords:
Coastal-water data assimilation
Phytoplankton
Chlorophyll
Primary production
Mediterranean Sea

ABSTRACT

The high spatial and temporal variability of biogeochemical features, induced by local dynamics and terrestrial and atmospheric inputs in shelf seas, are challenging issues for the implementation of data assimilation in these areas. The objective of this study is to integrate satellite ocean-colour observations with a coupled physical-biogeochemical model in order to improve the spatiotemporal descriptions of chlorophyll and other biogeochemical variables in the Mediterranean shelf seas. We adopted a specifically developed three-dimensional variational data assimilation scheme for the assimilation of satellite chlorophyll data. The non-homogeneous vertical component, the non-uniform and direction-dependent horizontal component of the background error covariance are the key features of the upgraded three-dimensional variational data assimilation scheme for shelf seas. The application of the new assimilation scheme significantly improves chlorophyll estimates in shelf seas, particularly in the representation of their spatial and temporal variability. Based on these results, we provide an estimate of the annual primary production of the Mediterranean basin.

1. Introduction

The physical and biogeochemical dynamics in shelf seas are characterised by large spatial and temporal variability due to their interactions with coastal and bottom morphology, and with boundary forcing. In particular, fronts and mixing associated with freshwater runoff, internal waves, tides and upwelling processes deeply affect the physical dynamics of shelf seas at spatial scales ranging from 10 m to more than 100 km (Denman and Powell, 1984; Mann and Lazier, 2005).

Understanding the biogeochemical dynamics in shelf seas is crucial for defining the environmental status of coasts and for supporting blue growth initiatives (She et al., 2016). Furthermore, an improved shelf-seas description results in a more consistent picture of basin-scale biogeochemical dynamics. Observations (both in situ and remote) and models can provide descriptions of shelf marine biogeochemistry at different spatial and temporal scales. Large datasets of in situ observations have been used to analyse the interaction between shelf-seas biogeochemical dynamics and physical processes at different scales and locations (e.g., in the European Sea: Arin et al., 2013; Cossarini et al., 2012; Guadayol et al., 2009; Mozetič et al., 1998; Romero et al., 2014; Solidoro et al., 2009; Varela et al., 2010) and long-term variability and trends (Giani et al., 2012; Harding et al., 2016; Kuosa et al., 2017; Lynch et al., 2014; Mozetič et al., 2010; Qiao et al., 2017; Rydberg et al., 2006; Yunev et al., 2007; Zingone et al., 2010).

Satellite observations are regularly collected and can provide synoptic information at a relatively high spatial resolution, and chlorophyll concentrations can be derived from satellite ocean-colour observations using algorithms based on colour spectra analysis (Muralikrishna, 1984; Santoleri et al., 2008; Volpe et al., 2007). Satellite ocean colour has been widely used to evaluate and monitor the water quality and ecological status of shelf seas (Gohin et al., 2008; Harvey et al., 2015; Novoa et al., 2012), inter-annual trends (Colella et al., 2016; Loisel et al., 2017; Mélin et al., 2011; Terauchi et al., 2014), and the spatial and temporal variability of blooms and trophic regimes (Beltrán-Abaunza et al., 2017; Blondeau-Patissier et al., 2014; Carvalho et al., 2011; D' Ortenzio and Ribera d' Alcalà, 2009; Gaetan et al., 2016; Marchese et al., 2014; Mayot et al., 2016; Rinaldi et al., 2014).

Finally, numerical models can seamlessly cover three-dimensional spatial and temporal domains at different scales and can be used to investigate specific processes, such as phytoplankton bloom and production dynamics and the effects of physical forcing on them (Campbell

* Corresponding author.
E-mail addresses: ateruzzi@inogs.it (A. Teruzzi), gbolzon@inogs.it (G. Bolzon), ssalon@inogs.it (S. Salon), plazzari@inogs.it (P. Lazzari), csolidoro@inogs.it (C. Solidoro), gcossarini@inogs.it (G. Cossarini).

https://doi.org/10.1016/j.ocemod.2018.09.007
Received 11 September 2018; Accepted 23 September 2018
Available online 06 October 2018

et al., 2013; Crise et al., 1999; Ennet et al., 2000; Fraysse et al., 2013; Friedrichs and Hofmann, 2001; Holt et al., 2012; Reboreda et al., 2014; St-Laurent et al., 2017; Tsiaras et al., 2014), as well as eutrophication (Nobre et al., 2005; Picart et al., 2015), hypoxia (Da et al., 2018; Meier et al., 2017; Testa et al., 2014), and assessment of carbon fluxes (Arruda et al., 2015; Cossarini et al., 2015; Hofmann et al., 2011; Melaku Canu et al., 2015).

None of these observations or models are without limitations. In situ data are point observations sparse in space and time with intrinsic representativeness error (Dowd et al., 2014), and they are thus unable to provide a basin-wide perspective; cloud cover limits the continuity of satellite data, which anyway do not provide information under the sea surface. Both in situ and satellite observations are affected by measurement error, and satellite estimates of chlorophyll also suffer from the uncertainty associated with the algorithm formulation (Volpe et al., 2012). On the other hand, models are affected by the approximations of their formulation (Cossarini. et al., 2009), the uncertainty associated with their parameters (Cossarini and Solidoro, 2008; Solidoro et al., 2003) and their boundary and initial conditions (Pastres et al., 1999), by numerical errors due to their discrete spatial and temporal resolution and the associated unresolved dynamical scales (Edwards et al., 2015).

The integration of models and observations using data assimilation schemes (DA) has been demonstrated to be a powerful tool in coupling different sources of information to obtain a better description of biogeochemical status and evolution. A number of recent applications have shown that data assimilation of satellite observations can be successfully applied in biogeochemistry to provide insight into different processes. Descriptions of the chlorophyll seasonal cycle, as well as investigations of vertical chlorophyll dynamics, carbon fluxes and hypoxia, have been provided by models that integrate a DA scheme for satellite observations (Ciavatta et al., 2014; Ciavatta et al., 2016; Fontana et al., 2009, 2010, 2013; Ford and Barciela, 2017; Ford et al., 2012; Hu et al., 2012; Kalaroni et al., 2016; Shulman et al., 2013; Song et al., 2016a; Teruzzi et al., 2014; Tsiaras et al., 2014). Some of the works above mentioned are focused on or include also shelf areas (Ciavatta et al., 2014,2016; Fontana et al., 2009; Fontana et al., 2010, 2013; Hu et al., 2012; Shulman et al., 2013; Song et al., 2016a). In the present work, we provide an example of how remote sensing observations on shelf areas can be efficiently integrated in a basin-scale model (which includes shelf and open sea areas) to improve the description of the biogeochemistry in shelf seas in the context of three-dimensional variational (3DVAR) data assimilation. The application of DA in coastal waters implies the development of a specific approach, because coastal marine biogeochemistry is strongly affected by local dynamics and inputs. Indeed, it is not straightforward that an open-sea assimilation scheme provides reliable results in coastal waters (Fontana et al., 2013). In Ciavatta et al. (2014) a lower decorrelation radius is applied at depth lower than 40 m. However simple, it is a practical approach to account for the specific features of coastal waters.

Here, the existing 3DVAR data assimilation scheme (Teruzzi et al., 2014), coupled with the OGSTM-BFM model (OGS Tracer Model – Biogeochemical Flux Model; Lazzari et al., 2012, 2016), has been specifically upgraded to assimilate remote observations in shelf seas. Independent in situ data have been used to provide a comprehensive estimate of the uncertainty of the model simulations produced using the new DA scheme. Furthermore, we provide an estimate of the integrated primary production at the basin scale, including shelf seas (which updates the one given in Lazzari et al., 2012).

The paper is organised as follows. Section 2 presents the details of the 3DVAR methods and the upgrades dedicated to shelf-seas assimilation; the OGSTM-BFM model and the observation datasets are also presented in Section 2. The results and validation of the assimilation run of the Mediterranean Sea, along with primary production estimations, are reported in Section 3. Finally, Section 4 and 5 provide the discussion and conclusions, respectively.

2. Material and methods

2.1. The CMEMS Mediterranean biogeochemical model system

The 3DVARBIO-OGSTM-BFM coupled biogeochemical model system consists of three major components: a transport model, OGSTM (Lazzari et al., 2012; Lazzari et al., 2010); a biogeochemical model, BFM (Cossarini et al., 2015; Lazzari et al., 2012, 2016; Vichi et al., 2007, and references therein); and a 3DVAR data assimilation scheme (3DVAR-BIO; Teruzzi et al., 2014). This model system is currently implemented with assimilation of open sea satellite chlorophyll within the Mediterranean component of the European Copernicus Marine Environment Monitoring Services (CMEMS) and operationally provides analysis/forecast and reanalysis products for the biogeochemistry of the Mediterranean Sea.

In the present application, we adopt the transport OGSTM model, a modified version of the OPA 8.1 transport model (Foujols et al., 2000), which resolves the advection, vertical diffusion and sinking terms of the tracers (i.e., biogeochemical variables). The mesh-grid is based on a $1/16^{\circ}$ longitudinal scale factor and a $1/16\cos(\varphi)$ latitudinal scale factor. The vertical mesh-grid accounts for 72 non-uniform vertical z-levels, in which there are 25 in the first 200 m depth, 31 between depths of 200 and 2000 m, and 16 below a depth of 2000 m. The minimum resolved depth is at the first level and is equal to 3 m. The temporal scheme of OGSTM is an explicit forward time scheme for the advection and horizontal diffusion terms, whereas an implicit time step is adopted for the vertical diffusion term.

The physical dynamics (i.e., temperature, salinity, velocity, and diffusivity fields, in addition to surface data for solar shortwave irradiance and wind stress) that are coupled off-line with biogeochemical processes are precomputed using NEMO3.4 coupled with OceanVar assimilation (Dobricic and Pinardi, 2008) and are available through the CMEMS catalogue (Simoncelli et al., 2014). The physical forcing fields have daily frequency, and they are linearly interpolated at the computational time step of the OGSTM-BFM model (30 min).

The features of the biogeochemical reactor BFM (Biogeochemical Flux Model) have been chosen to target the energy and material fluxes through both “classical food chain” and “microbial food web” pathways (Thingstad and Rassoulzadegan, 1995) and to take into account the co-occurring effects of multi-nutrient (i.e., carbon, nitrogen, phosphate, silicate) interactions. Both of these factors are very important in the Mediterranean Sea, wherein microbial activity fuels the trophodynamics of a large part of the system throughout much of the year and both phosphorus and nitrogen can in principle play limiting roles (Béthoux et al., 1998; Krom et al., 1991).

The BFM model includes nine plankton functional types (PFTs). Heterotrophic PFTs consist of carnivorous and omnivorous mesozooplankton, bacteria, heterotrophic nanoflagellates and microzooplankton. The autotrophic PFTs are diatoms, flagellates, picophytoplankton, and dinoflagellates. Internal contents of carbon, nitrogen, phosphorous, chlorophyll and silicon (only for the diatoms PFT) are dynamically simulated, summing up on 17 state variables needed to represents the four phytoplankton functional types. The model is fully described in Lazzari et al. (2012), (2016), where it was corroborated for chlorophyll, primary production and nutrients in the Mediterranean Sea in a 1998–2004 simulation. The BFM model is also coupled to a carbonate system model (Cossarini et al., 2015) in order to simulate the dynamics of alkalinity, pH, dissolved inorganic carbon and CO_2 fluxes at the air-sea interface.

In the CMEMS workflow, which is applied for both analysis/forecast and reanalysis simulations, the data assimilation of surface satellite chlorophyll concentration data is performed every seven days using a 3DVAR scheme (3DVAR-BIO; Teruzzi et al., 2014), which updates the four phytoplankton functional groups that are included in the BFM. 3DVAR methods represent a feasible and efficient framework for assimilation in oceanographic applications because they allow to properly

design the key aspects of assimilation problems, such as the background and observation error covariance matrix, thus mantaining computational costs affordable (Dowd et al., 2014; Edwards et al., 2015).

The 3DVAR-BIO assimilation scheme (Teruzzi et al., 2014) computes the analysis status, $\mathbf{x}_a$, from the minimization of a cost function J, in which the forecast and observations are weighted by their respective error covariance matrices. In the present formulation the assimilation updates all the 17 phytoplankton variables. The cost function can be written as a function of the increment $\delta_{\mathbf{x}}$, which is defined as the difference between the analysis $\mathbf{x}_a$ and the forecast produced by the model $\mathbf{x}_f$ ($\delta_{\mathbf{x}} = \mathbf{x}_a - \mathbf{x}_f$). At a generic assimilation step, the cost function is defined as follows:

$$J(\delta\mathbf{x}) = \frac{1}{2}\delta\mathbf{x}^{\mathrm{T}}\mathbf{B}^{-1}\delta\mathbf{x} + \frac{1}{2}(\mathbf{d} - \mathbf{H}\delta\mathbf{x})^{\mathrm{T}}\mathbf{R}^{-1}(\mathbf{d} - \mathbf{H}\delta\mathbf{x}), \quad (1)$$

where $\mathbf{B}$ and $\mathbf{R}$ are the covariance matrices for the background and observational errors, respectively; $\mathbf{H}$ is the Jacobian of the observation operator ($\partial h/\partial x$) which sums the surface chlorophyll contributes from the four phytoplankton functional types; and $\mathbf{d}$ is the difference between observations $\mathbf{y}$ and model results ($\mathbf{d} = \mathbf{y}\text{-}\mathbf{H}(\mathbf{x})$, and is referred as the innovation vector). After undergoing opportune transformations, the cost function can be written as a function of a vector $\mathbf{v}$ (with $\delta\mathbf{x} = \mathbf{V}_b\mathbf{V}_h\mathbf{V}_v\mathbf{v}$):

$$J(\delta\mathbf{x}) = \frac{1}{2}\mathbf{v}^{\mathrm{T}}\mathbf{v} + \frac{1}{2}(\mathbf{d} - \mathbf{H}\mathbf{V}_b\mathbf{V}_h\mathbf{V}_v\mathbf{v})^{\mathrm{T}}\mathbf{R}^{-1}(\mathbf{d} - \mathbf{H}\mathbf{V}_b\mathbf{V}_h\mathbf{V}_v\mathbf{v}). \quad (2)$$

In Eq. (2), the forecast (or background) covariance matrix $\mathbf{B}$ is approximated as $\mathbf{B} = \mathbf{V}\,\mathbf{V}^T$, where $\mathbf{V}$ is a mapping operator that, following the approach of Dobricic and Pinardi (2008), is decomposed into a sequence of operators that account for different components of the error covariance. In particular, $\mathbf{V} = \mathbf{V}_b\,\mathbf{V}_h\,\mathbf{V}_v$, which are the biogeochemical, horizontal, and vertical operators, respectively. The solution of the minimization is the vector $\mathbf{v}$, whose dimension is defined by the definition of the vertical operator $\mathbf{V}_v$ (i.e., a set of Empirical Orthogonal Functions).

The increments are then applied to the 3D fields of the 17 biogeochemical variables, which describe the phytoplankton functional types, through the application of $\mathbf{V}_h$ (i.e., a Gaussian recursive filter) and $\mathbf{V}_b$ (i.e., a biogeochemical covariance operator). The operator $\mathbf{V}_b$ is a biomass covariance operator, which preserves the ratios among phytoplankton functional types and their internal quotas with additional criteria to maintain the optimal phytoplankton growth rate based on the optimal nutrient to carbon internal quota (Teruzzi et al., 2014). Finally, the $\mathbf{V}_b$ operator includes also a post-processing procedure, which replaces the negative chlorophyll values with a small positive value (10^{-4} mg chl/m^3) and change accordingly the components of each PFT, in order to avoid any negative values in the PFT components. The effect of this correction is negligible since the negative values are low (i.e., order of -10^{-2} or closer to zero), in small number (nearly 5.5% of the cases) and located mainly below the photic zone where chlorophyll concentrations are low and the intensity of phytoplankton dynamics is reduced.

2.2. Chlorophyll estimates from satellite data

In recent years, new algorithms have been developed to provide shelf-seas ocean-colour products (Le Traon et al., 2015). The surface chlorophyll concentration used in the assimilation scheme is a product of the CMEMS Ocean Colour Thematic Assembly Centre (OC-TAC) service obtained using remote sensing reflectance (Rrs) spectra. Rrs data are produced for CMEMS by the Plymouth Marine Laboratory (PML) using the ESA-CCI processor.

Estimates of chlorophyll for the Mediterranean Sea are provided by the Global Ocean Satellite group (GOS) of the Institute of Atmospheric Sciences and Climate (ISAC) within the Italian National Research Council (CNR), using two different algorithms: MedOC4 (Volpe et al., 2007) for case 1 water and AD4 (D'Alimonte and Zibordi, 2003) for case 2 water (Colella et al., 2016). Water is classified as case 1 or case 2 water using the method proposed by D'Alimonte et al. (2003) based on the comparison of the satellite spectrum with the average spectral signature of the water type obtained from in situ measurements. Full basin estimates of chlorophyll concentration based on the approach proposed by D'Alimonte et al. (2003) are operationally provided by CMEMS along with their validation (OCEANCOLOUR_MED_CHL_L3_NRT_OBSERVATIONS_009_040, http://marine.copernicus.eu/services-portfolio/access-to-products/?option=com_csw&view=details&product_id=OCEANCOLOUR_MED_CHL_L3_NRT_OBSERVATIONS_009_040). For the present application, daily chlorophyll concentrations at a spatial resolution of 1 km have been interpolated at 1/16° and temporally aggregated using a seven-day average to increase the spatial coverage of the assimilated field without losing excessive details about the temporal evolution of the surface chlorophyll field.

The error covariance matrix for the observations ($\mathbf{R}$ in Eq. (1)) has been assumed to be diagonal (excluding error covariance between observations), and monthly varying variances have been adopted. For each grid-point, the error variance has been estimated as the variance of the multiannual (1999–2015) time series of chlorophyll concentration produced by GOS-ISAC group using the algorithm above described. In our pragmatic approach, higher observation errors are attributed to areas with higher variabilities (as discussed in Teruzzi et al., 2014). This approach differs from the usual one that sets the observation error of ocean-colour data as proportional to the observed chlorophyll concentration (Fontana et al., 2013; Hu et al., 2012; Song et al., 2016a; Tsiaras et al., 2017). However, other approaches include, for instance, the use of an observation error derived from the standard deviation associated to the ocean-colour products (Ciavatta et al., 2016) or from an observation-based ensemble (Shulman et al., 2018).

2.3. Independent in situ dataset for validation

The in situ dataset consists of measurements of chlorophyll, nitrate and phosphate along the Italian coast (Table 1 and Fig. 1) at a maximum shore distance of 3 km, provided by the Italian National Institute for Environmental Protection and Research (ISPRA) (SINTAI dataset; http://www.sintai.isprambiente.it/). Data were collected almost regularly at monthly or higher frequencies by different regional environmental agencies in 2013; these data were then quality processed by ISPRA.

2.4. Upgrade of the 3DVAR-BIO assimilation scheme

The upgraded elements of the new version of the 3DVAR-BIO scheme, which is used for the assimilation of shelf-seas observations, are the horizontal ($\mathbf{V}_h$) and vertical ($\mathbf{V}_v$) operators, which have been modified to account for the specific dynamics of error propagation in the shelf seas.

2.4.1. Upgrade of the vertical operator V_v

The vertical operator ($\mathbf{V}_v$) provides the error covariance in the vertical direction. It comprises a set of profiles of chlorophyll error

Table 1
ISPRA dataset: subbasins with available observations, numbers of stations and observations of the quantities used for validation.

	No. of stations	No. of observations	Subbasins with observations
Chlorophyll [mg/m^3]	129	1666	ADN, ADS, ION, TYR
Nitrate [mmol/m^3]	122	788	ADN, ADS, ION, NWM
Phosphate [mmol/m^3]	61	569	ADN, NWM

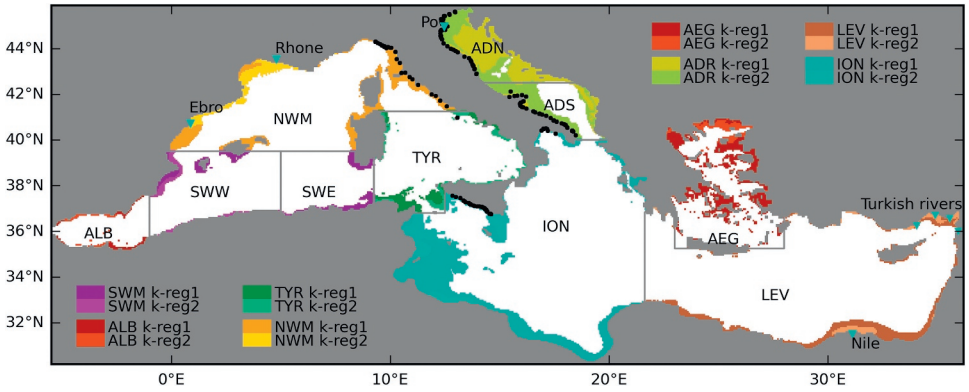

Figure 1. Map of the Mediterranean Sea with delimitations of subbasins (ALB: Alboran Sea; SWW: South West Western Mediterranean, SWE: South West Eastern Mediterranean; NWM: North West Mediterranean; TYR: Thyrrhenian Sea; ADN: Northern Adriatic Sea; ADS: Southern Adriatic Sea; ION: Ionian Sea, LEV: Levantine Sea; AEG: Aegean Sea). Stations of in situ measurements used for validation are identified by black dots along the Italian coast. Colours in areas with depths of less than 200 m represent the *k*-mean classification (*k*-reg1 and *k*-reg2). Cyan triangles indicate the locations of main rivers.

covariances that are obtained using an EOF (empirical orthogonal function) decomposition of a dataset of vertical chlorophyll profiles. To account for differences in the vertical biogeochemical dynamics of shelf and open sea areas, a dedicated $\mathbf{V}_v$ operator has been designed for the shelf seas. The depth of 200 m is chosen as the threshold between shelf and the open sea (Fig. 1), according to previous applications in Mediterranean Sea (Gazeau et al., 2004; Lazzari et al., 2012; Teruzzi et al., 2014).

As described in Teruzzi et al. (2014), in the open sea (i.e., at depths greater than 200 m), the $\mathbf{V}_v$ operator consists of a set of vertical EOF profiles defined for each month and for each subbasin of Fig. 1. The same temporal and spatial approach was applied to the shelf seas; however, a much finer spatial resolution was chosen in order to account for the specificity of local features along the Mediterranean coast. In particular, a *k*-means analysis, based on the time evolution of the chlorophyll field provided by the 1999–2015 CMEMS reanalysis (Teruzzi et al., 2016), identified two *k*-regions for each shelf area of the 10 subbasins (Fig. 1). Details on the *k*-means approach are provided in Appendix A.

The *k*-region subdivision reveals that, within a given subbasin shelf area, the two *k*-regions can distinguish the areas (*k*-reg2) affected by important river run-off (i.e., the Ebro and Rhone rivers for the North Western Mediterranean Sea (NWM), the Nile and Turkish rivers for the Levantine Sea (LEV), and the Po and other minor South-Eastern Adriatic rivers for the Adriatic Sea (ADR)) or similar local inputs (i.e., the Dardanelles for the Aegean Sea (AEG)) from the areas (*k*-reg1) that are far from the river mouths. The evolution of the total variance of the error (Fig. 2) shows higher values in late winter or spring in the *k*-regions that are affected by rivers (*k*-reg2) in the NWM, LEV and ADR, which is consistent with the hypothesis that important differences in chlorophyll dynamics are triggered by land forcing along the coast of the subbasins. In the Ionian Sea (ION), which is characterised by the absence of relevant riverine inputs, the two *k*-regions are patchily distributed and are distinguished only by their summer variance, which is higher in the Gulf of Gabes and along the African coast.

The EOF decomposition was applied to the weekly chlorophyll anomaly profiles within each *k*-region and month in order to obtain sets of profiles of the vertical error covariance that are specific to different parts of the Mediterranean shelf seas. Thus, the result of the EOF decomposition is a set of eigenvectors (chlorophyll vertical profiles) and associated eigenvalues for each *k*-region in shelf seas and each subbasin in open sea. Each set of eigenvectors and associated eigenvalues represent the vertical error covariance for each subbasin or *k*-region of the Mediterranean Sea. Finally, according to Desroziers et al. (2005), a tuning procedure based on the surface observation error covariance and the difference between observation and model before the assimilation **d** is used to compute the eigenvalues of the EOF profiles at a local scale (i.e., at each grid point). The mean quadratic innovation $E[\mathbf{dd}^{\mathrm{T}}]$ is defined as being equal to the sum of the observation error variance **R** and the background error variance at the surface, thus tuning the eigenvalues α_i of the EOFs at each grid point as follows:

$$E[\mathbf{dd}^T] = \mathbf{R} + \mathbf{H}(\sum \alpha_i \mathbf{E}_i)(\sum \alpha_i \mathbf{E}_i)^T \mathbf{H}^T, \quad (3)$$

where the second term in the right-hand side of the equation is the background error variance at the surface, as described by the EOF, and $\mathbf{E}_i$ are the eigenvectors of the EOFs. In the evaluation of α_i it has been

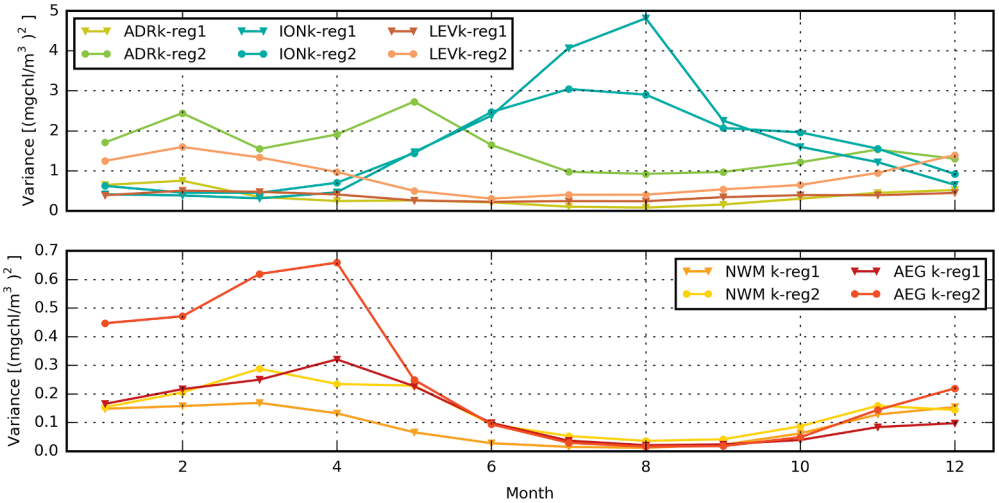

Fig. 2. Time series of mean monthly surface variance of chlorophyll [(mg chl/m^3)^2] in *k*-reg1 and *k*-reg2 of selected subbasins (Fig. 1). Top panel: Adriatic (ADN and ADS), Ionian (ION) and Levantine Seas (LEV); bottom panel: North Western Mediterranean (NWM) and Aegean Seas (AEG).

imposed that the background error variance is at least equal to half of the observation error variance, in order to guarantee the effective assimilation of satellite observations.

As a result, the $\mathbf{V}_v$ operator of the Mediterranean Sea consists of a set of EOF profiles for each grid point that share a common shape within each subbasin in open sea and within each *k*-region in shelf seas.

2.4.2. New horizontal operator V_h

The operator $\mathbf{V}_h$, which describes the horizontal error covariance, is based on a recursive Gaussian smoother whose effect is regulated by the correlation radius length scale L (Dobricic and Pinardi, 2008). In the open sea, L is set to 10 km (Teruzzi et al., 2014), which is within the order of magnitude of the Mediterranean Sea mesoscale (Lionello, 2012) In shelf-seas, where the morphology and local physical features can produce sharp gradients of biogeochemical fields, L differs in its longitudinal (L_x) and latitudinal (L_y) directions. In particular, constant in time values of L_x and L_y were computed for all shelf-seas grid-points proportionally to the inverse of the surface salinity gradient components along the longitude and the latitude ($\nabla_x S(x,y)$ and $\nabla_y S(x,y)$), respectively, as follows:

$$L_x(x,y) = \frac{\langle \nabla_x S \rangle}{\nabla_x S(x,y)} L, \tag{4}$$

$$L_y(x,y) = \frac{\langle \nabla_y S \rangle}{\nabla_y S(x,y)} L, \tag{5}$$

where $\langle \nabla_i S \rangle$ is the mean salinity gradient component along x and y over the Mediterranean Sea. Surface salinity can be considered to be a signature of local dynamics in shelf seas, and it can be assumed that more local processes (i.e., those with a smaller correlation radius) correspond to higher salinity gradients. The surface salinity field used to estimate the length of the correlation radius is based on the 1990–2015 mean value of the CMEMS Mediterranean Sea physics reanalysis (Simoncelli et al., 2014).

The correlation lengths calculated using the salinity gradient (Fig. 3) are nearly one-third the size of the open sea correlation length in the northern and southeastern Adriatic Sea, the northeastern Aegean Sea (AEG), the Gulf of Gabes, and other more patchy areas along the Mediterranean coast. In these regions, the reduced correlation length reflects the reduced horizontal propagation of the increments provided by the data assimilation. Other areas, e.g., the Italian shores of the Tyrrhenian Sea, the western side of the Adriatic Sea (in the longitude direction), the Gulf of Libya, the Israeli coast and the southern Aegean Sea (in the latitude direction), show correlation radii that are larger than the average open sea value, thus reflecting the fact that in areas with smooth salinity gradients, the spread of the assimilation updates is higher.

2.5. Setup of the simulations

In the present paper, the following three simulations are compared: FullDA, OpenDA and NoDA. The first two runs differs in terms of $\mathbf{V}_v$, $\mathbf{V}_h$ and observation operators. The observation operator in OpenDA is defined in order to assimilate the open sea observations only (i.e., where water depth is higher than 200 m). Whereas, in FullDA it has been designed in order to assimilate all the observations (both in shelf and open sea). Moreover, FullDA uses the upgraded $\mathbf{V}_v$ and $\mathbf{V}_h$ operators. A reference run without assimilation (NoDA) completes the simulation list.

The simulations cover the period from January to December 2013, because the availability of the ISPRA in situ observation dataset in 2013 allows us to quantitatively evaluate the impact of the assimilation of shelf-seas data. The simulations share the same setup, which is based on the official CMEMS Mediterranean Analysis & Forecast system (Bolzon et al., 2017). In particular, physical forcing is provided by CMEMS products (Simoncelli et al., 2014), while climatological biogeochemical boundary conditions are set for Gibraltar Strait, the Dardanelles, rivers and atmosphere forcing. Nutrient concentrations in the Atlantic buffer zone are relaxed to the seasonally varying profiles derived from climatological MEDAR-MEDATLAS data measured outside Gibraltar. Climatologies of nutrient loads from rivers and other coastal nutrient sources were based on the reconstruction of the spatial and temporal variability in water discharge estimated using the method described by Ludwig et al. (2009). Atmospheric deposition rates of inorganic nitrogen and phosphorus are defined according to the synthesis proposed by Ribera d' Alcalà et al. (2003). Initial conditions are given after the

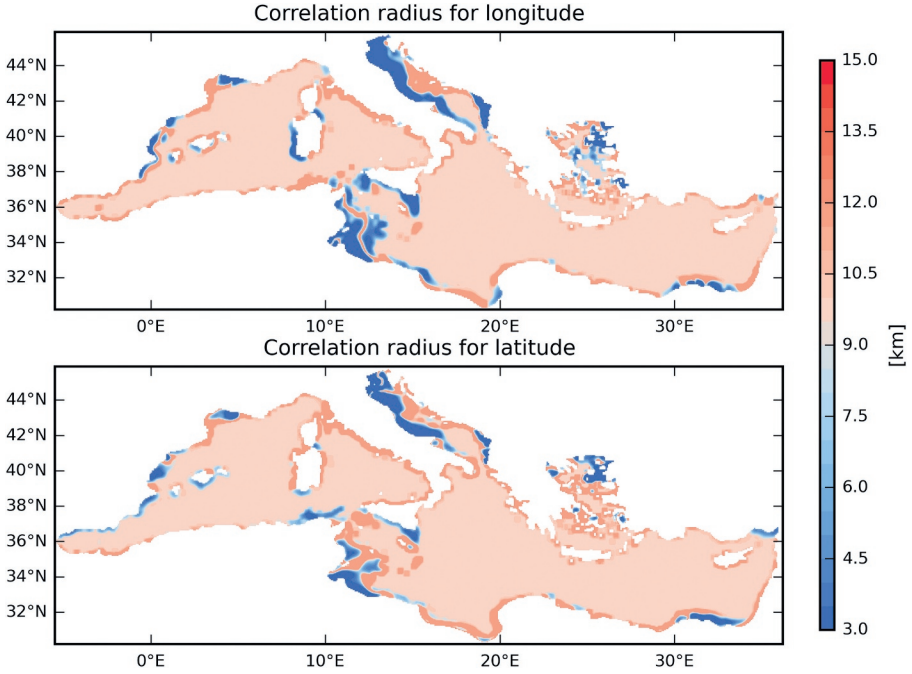

Fig. 3. Maps of correlation radius length scales L_x and L_y Eqs. (4) and ((5)).

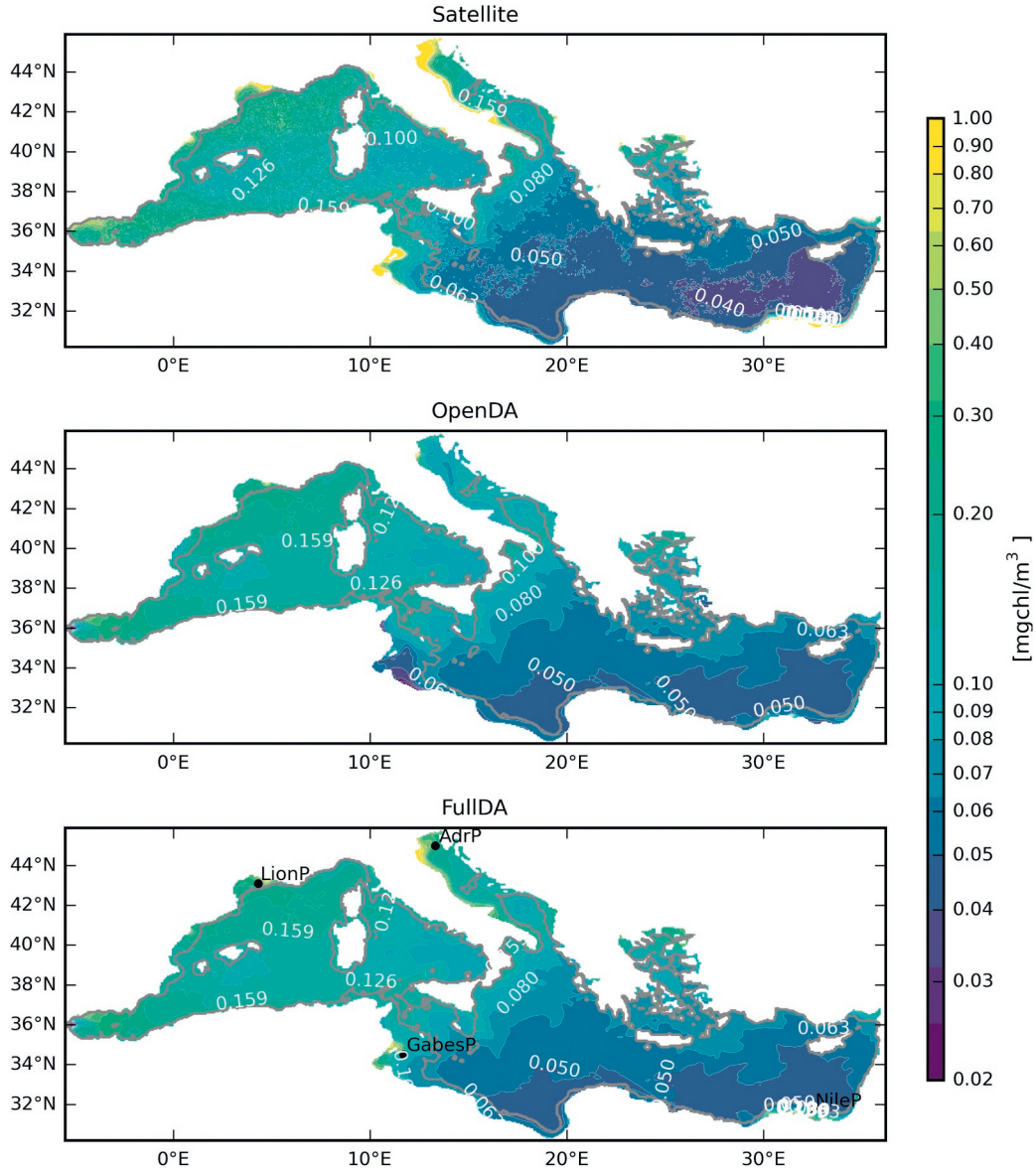

Fig. 4. Maps of mean surface chlorophyll concentrations in the year of simulation (2013): satellite (top panel), OpenDA (middle panel), and FullDA (bottom panel). OpenDA and FullDA maps have been evaluated regardless to satellite coverage. The grey line defines the areas with depths of less than 200 m. The time series of Fig. 5 have been extracted at the points defined in the bottom panel (AdrP, LionP, GabesP, and NileP).

spin-up of a 14-year-long run of biogeochemical reanalysis (CMEMS reanalysis; Teruzzi et al., 2016). Regarding the assimilation, the two assimilation setups (i.e., OpenDA and FullDA) compare the present one (Bolzon et al., 2018) and the previous CMEMS Mediterranean Analysis & Forecast system versions (Bolzon et al., 2017.

3. Results

3.1. Comparison between FullDA and OpenDA

The main effect of FullDA is a general increase in the surface chlorophyll concentrations of shelf seas, which is consistent with the high chlorophyll concentrations observed by satellite (Fig. 4 and Table 2). The FullDA increase in mean chlorophyll values is more evident in the subbasins with a wide continental shelf, such as the Adriatic Sea (ADN and ADS) and the Gulf of Gabes in the Ionian Sea (ION). The mean chlorophyll concentration in FullDA is higher than in OpenDA by nearly 50% in the Mediterranean shelf seas, which is consistent with the assimilation of shelf-seas satellite chlorophyll applied in FullDA and not in OpenDA

In the Adriatic and Ionian shelf-seas the relative difference between FullDA and OpenDA is nearly equal to 100% and 60%, respectively. In these areas, the effects of shelf-seas assimilation include both a significant increase in the surface chlorophyll concentration and a modification of its pattern. In the Adriatic Sea, the highest concentrations of FullDA are located in the northern Adriatic Sea and along the Italian coast, thus providing an east-west gradient of chlorophyll that substantially differs from the results obtained by OpenDA but is consistent with satellite observations and the well-known chlorophyll features of the subbasin (Mélin et al., 2011; Zavatarelli et al., 2000).

In the Gulf of Gabes, the increments applied in FullDA yield maximum chlorophyll concentrations in the eastern part of the area, which is consistent with satellite observations (Fig. 4) but is opposite to the results of OpenDA. Also, the chlorophyll concentrations in LEV and AEG, near the Nile mouth and the Dardanelles, are significantly impacted in FullDA (Fig. 4). In shelf seas the mean chlorophyll concentration is increased by FullDA by nearly 70% and 30% in LEV and AEG, respectively. The increase of the mean shelf-sea chlorophyll in LEV is relevant despite the relative small extension of its shelf sea, and

Table 2
Percentage of shelf seas (with depths of less than 200 m) and shelf-seas spatial and temporal mean of first-layer chlorophyll (mean) in FullDA, OpenDA and NoDA, and their relative differences for each subbasin and for the whole Mediterranean Sea (MED).

Sub-basin	Shelf seas	Mean FullDA	OpenDA	NoDA	(FullDA-OpenDA)/OpenDA	(FullDA-NoDA)/NoDA	(OpenDA-NoDA)/NoDA
ALB	9%	0.244	0.226	0.156	8%	56%	45%
SWW	9%	0.161	0.137	0.118	18%	36%	16%
SWE	9%	0.156	0.146	0.117	7%	33%	25%
NWM	18%	0.212	0.179	0.165	18%	28%	8%
TYR	11%	0.145	0.132	0.111	10%	31%	19%
ADN	94%	0.246	0.116	0.107	112%	130%	8%
ADS	49%	0.210	0.112	0.099	88%	112%	13%
AEG	25%	0.139	0.108	0.088	29%	58%	23%
ION	19%	0.114	0.072	0.067	58%	70%	7%
LEV	8%	0.106	0.063	0.064	68%	66%	−2%
MED	17%	0.163	0.108	0.097	51%	68%	11%

is due to the large positive increments applied by DA in the Nile mouth region (Fig. 4). Indeed, the climatological inputs used for the Nile river do not account for the positive trend of chlorophyll concentration in the area. This trend has been documented by Colella et al. (2016), and is related to the increase of the Egypt industrial capacity.

The differences between OpenDA and NoDA highlights that the open-sea assimilation affects also the chlorophyll concentration in the shelf-seas (Table 2). The open-sea assimilation increments are propagated to the shelf seas due to the effect of $\mathbf{V}_h$ operator and of the transport processes during model integration. As a result, the OpenDA shows increments in the shelf seas that have the same sign of those applied in open sea close to the shelf. The sign of the increments is mainly positive, but an exception is shown for LEV where open-sea increments are mainly negative (not shown) and thus also in the shelf-seas. Even if with some exceptions, generally, the higher the extent of the shelf area is compared to the sub-basin area, the lower the OpenDA impacts on shelf sea. The differences between FullDA and NoDA are at least doubled compared to those of OpenDA in most of the subbasins.

FullDA produces a significant increase in the spatial variability of simulated chlorophyll in shelf seas (74% increase in the whole Mediterranean Sea; Table 3). The mean spatial standard deviation in shelf seas of FullDA is significantly higher than that of the OpenDA simulation in all the subbasins, especially in ADN, ADS, ION and LEV (Table 3), which indicates that the assimilation of satellite data increased the simulated variability on a local scale and on areas interested by patchy processes.

Examples of chlorophyll time series in four near-shore grid-points are shown in Fig. 5. In all of the points, which are representative of the chlorophyll dynamics in the four shelf areas, the effects of the assimilation of shelf-seas satellite chlorophyll of FullDA are clearly detectable. Indeed, the FullDA time series are closer to the satellite observations in terms of weekly signal and monthly variability (black solid line in Fig. 5). In particular, FullDA exhibits relevant effects at the beginning and at the end of the year, when the FullDA concentrations are significantly higher than the OpenDA concentrations (except for the LionP time series).

Table 3
Shelf-seas temporal mean over the simulation period of the spatial standard deviation (Spatial STD) in FullDA and OpenDA and their percent difference (Diff = (FullDA-OpenDA)/OpenDA) for each subbasin and for the whole Mediterranean Sea (MED).

Sub-basin	Spatial STD FullDA	OpenDA	Diff
ALB	0.147	0.133	10%
SWW	0.050	0.047	6%
SWE	0.048	0.042	14%
NWM	0.132	0.101	31%
TYR	0.050	0.042	19%
ADN	0.229	0.113	103%
ADS	0.108	0.042	157%
AEG	0.097	0.058	67%
ION	0.108	0.045	140%
LEV	0.101	0.042	140%
MED	0.153	0.088	74%

During spring and summer, three locations (i.e., AdrP, LionP and NileP, in several weeks from May to September) show a low persistence of the assimilation updates. After the assimilation, the chlorophyll concentrations of FullDA (daily model output in grey line in Fig. 5) tend to decrease towards the values simulated by the model without the shelf-seas assimilation (OpenDA), and FullDA simulation presents an artificial temporal variability at daily time scale. In these cases nearly 80% of the increments introduced by the assimilation is lost five days after the assimilation. Fig. 5 also shows that the increments applied by FullDA during summer are small in Gabes P and NileP (in June), thus indicating that in these cases, the time evolution of chlorophyll is already well-represented by the OpenDA model setup.

Using monthly climatological terrestrial inputs (e.g., nutrient load) as boundary conditions probably underestimates the effects of actual runoff events on triggering shelf-seas blooms. In FullDA, the assimilation of case 2 satellite chlorophyll observations can overcome the inadequacy of climatological local forcing conditions by acting directly on the state variables. Fig. 6 shows examples of the spring and autumn bloom events in the Adriatic Sea that are related to important terrestrial inputs from the Po river, which are efficiently corrected by FullDA. The low-salinity patterns (Fig. 6, left column) highlight the presence of important river runoff and consequent nutrient discharge in the area. The use of the climatological boundary conditions applied in the OpenDA results cannot be used to reproduce the effects of short-lasting and impulsive events on phytoplankton dynamics (Fig. 6, central column), whilst FullDA correctly simulates the presence of high chlorophyll concentration values that match the low-salinity patterns (Fig. 6, right column).

The computed time series of the spatial correlation between the salinity and chlorophyll patterns of OpenDA and FullDA in the northern Adriatic areas do not show a significant increase with FullDA (not shown). This is likely because small surface chlorophyll blooms may be triggered by very local hydrodynamic features whose temporal and spatial details are not fully captured by the physical forcing model. However, FullDA significantly improves the representation of wide blooms related to low-salinity events.

The spatial distribution of the DA increments of FullDA in shelf seas is related to the application of the non-uniform and non-isotropic horizontal operator $\mathbf{V}_h$. To evaluate its effect, we compared the differences in the assimilation results obtained using a uniform and isotropic correlation length (L = 10 km, "uniVh" case) and those obtained using the new $\mathbf{V}_h$ ("nonuniVh" case). The difference $\mathbf{d}_a$ between the satellite observations ($\mathbf{y}$) and the surface chlorophyll yielded by the assimilation

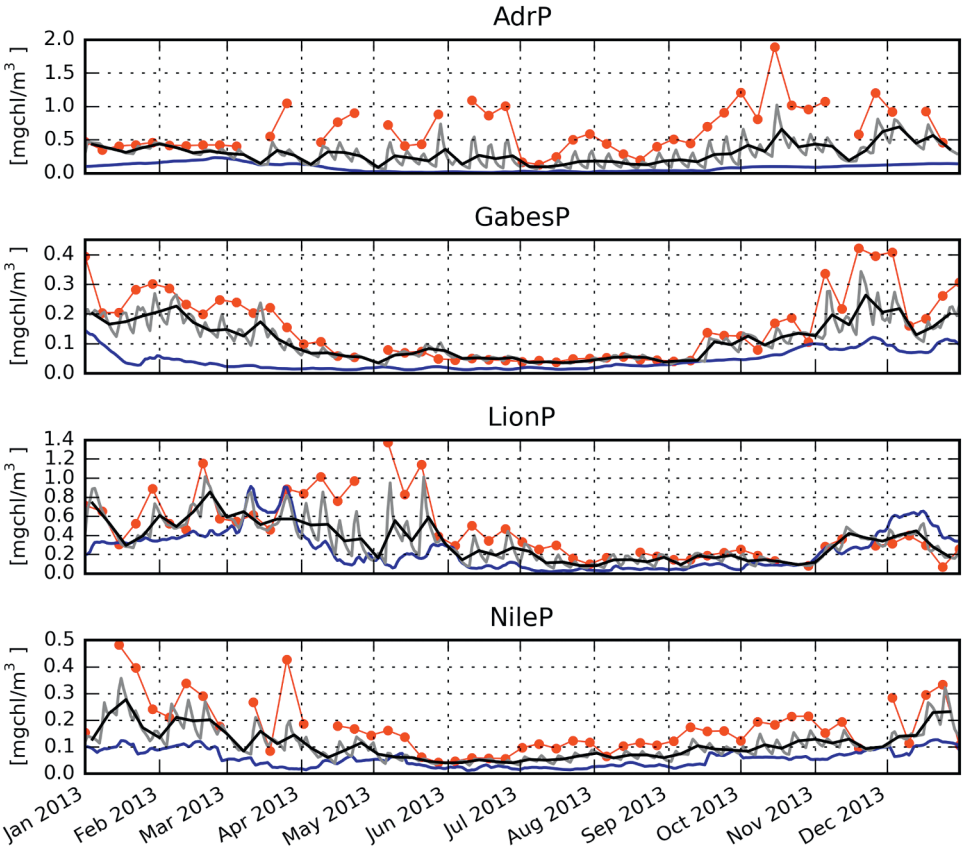

Fig. 5. Time series of surface chlorophyll concentrations in four points (locations in Fig. 4) for daily OpenDA (blue line), daily (grey line) and weekly (black line) FullDA, and satellite (red line and dots). Satellite time series are not continuous due to cloud cover. (For interpretation of the references to colour in this figure legend, the reader is referred to the web version of this article.)

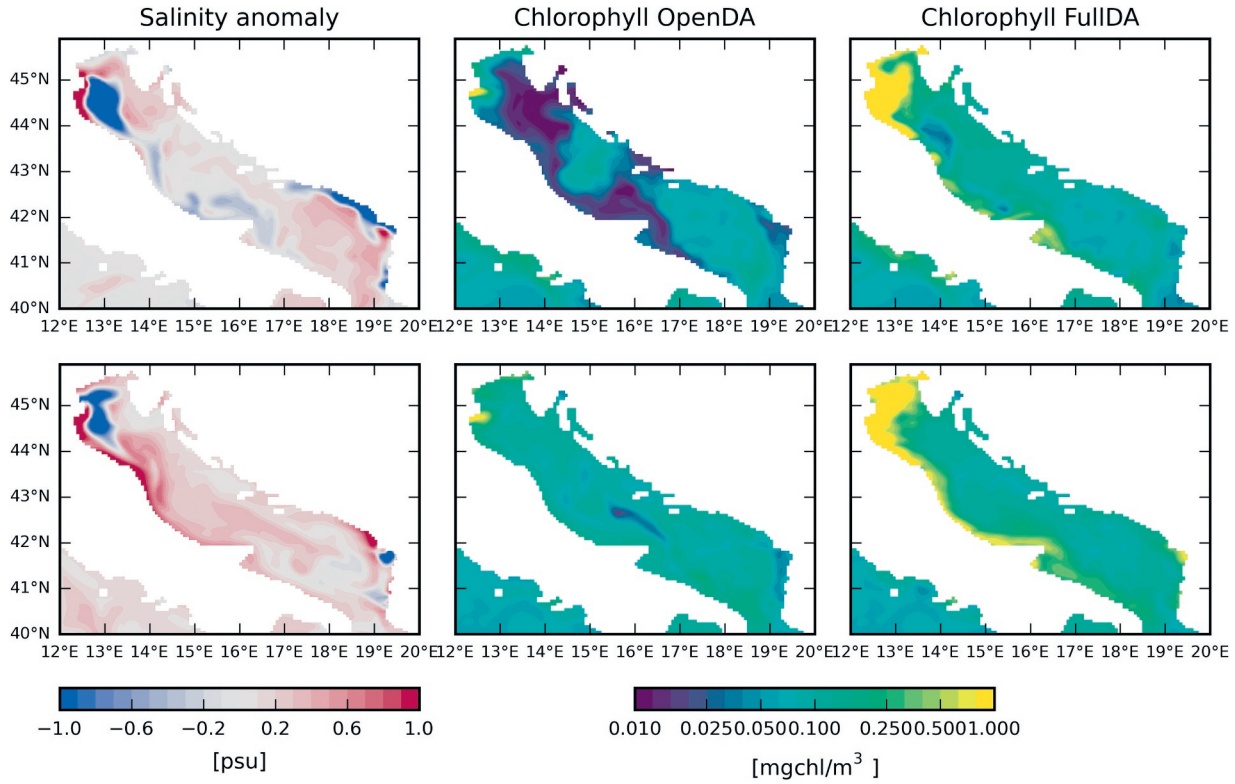

Fig. 6. Surface salinity anomaly [psu] and chlorophyll [mg chl/m^3] maps in the Adriatic Sea for 29 May (top panels) and 30 October (bottom panels).

Table 4
Root mean square (RMS) values of $\mathbf{d}_a$ (differences between observations and chlorophyll obtained after assimilation) for the uniVh and newVh cases and their percentage differences. Mean *x*- and *y*-components of the horizontal gradient of chlorophyll (Gradx and Grady, i.e., along longitude and latitude, respectively) evaluated as the spatial averages of the gradient at each grid-point in coastal areas with correlation radii along longitude (L_x) and latitutde (L_y) smaller than their respective open sea values. Gradient components have been computed by means of a finite difference scheme.

RMS of $\mathbf{d}_a$ [mg chl/m^3]			Chlorophyll gradient [mg chl/m^{3}deg] Gradx where $L_x < L$			Grady where $L_y < L$		
uniVh	nonuniVh	Difference	Sat	uniVh	nonuniVh	Sat	uniVh	nonuniVh
0.325	0.207	−36%	0.059	0.042	0.054	0.066	0.049	0.063

($\mathbf{x}_a$) was evaluated for these two cases. The root mean square (RMS) values of $\mathbf{d}_a$ in the Mediterranean shelf-seas (Table 4) show that the application of the new $\mathbf{V}_h$ operator produces an assimilated field that is closer to the observations than that obtained in the uniVh case. The highest reductions of the $\mathbf{d}_a$ RMS values are observed in the eastern subbasin (ADN, ADS, AEG, ION and LEV, not shown), which yield percentage differences ranging from −15% in ADS to −49% in ADN.

The use of two different correlation radii for longitude (L_x) and latitude (L_y) can affect the distribution of the assimilation increments in the horizontal plane. It is expected that the assimilation updates are more local and less smooth along one direction (*x* or *y*), where the relative correlation radius (L_x or L_y) is smaller than the reference value *L*. The fact that a lower correlation radius in shelf seas is essential to produce local small-scale features is demonstrated by the chlorophyll gradient computed where L_x or L_y are smaller than *L* in the uniVh, nonuniVh and satellite surface chlorophyll cases (Table 4). In the nonuniVh case, the chlorophyll gradient components are closer to the satellite values, thus indicating that the use of a smaller correlation radius for longitude or latitude reduces the smoothing of the solution in accordance with the high horizontal variability of satellite observations.

3.2. Validation using the in situ dataset

The improvement that is introduced by using DA to simulate chlorophyll in open sea areas has been shown by Teruzzi et al. (2014). Here, we compare the results of the FullDA and OpenDA simulations with independent in situ observations of chlorophyll and nutrient concentrations collected at the surface in the shelf areas of the ADN, ADS, ION, TYR and NWM subbasins (Fig. 1). Table 5 shows the mean bias (model results minus observations) and the root mean square difference (RMSD) values for the subbasins using available data from two 6-month periods, i.e., January to June (or semester “win-spr”) and July to December (or semester “sum-aut”).

The chlorophyll bias between observations and OpenDA is always negative, which means that the model results systematically underestimate the in situ observations. FullDA, which generally increases chlorophyll concentrations (Figs. 4 and 5), significantly reduces the bias in all subbasins. The largest improvements occur in ADN and ADS in both semesters and in TYR in win-spr. The RMSD is significantly improved in ADN and TYR in win-spr. In the sum-aut period, the RMSD decreases by 10% in ADN, remains almost unchanged in TYR and ION and slightly increases in ADS. The high positive increments towards satellite data in ADS during sum-aut induced by the shelf-seas assimilation change the sign of the bias and reduce its absolute value.

The comparison of the available observations of non-assimilated variables shows that FullDA has negligible influence on the bias and RMSD values of phosphate, while it affects those of nitrate (Table 5). The range of measured nitrate concentrations is very high, i.e., on the order of 10 mmol N/m^3 in ADN, 1 mmol N/m^3 in ADS and slightly less than 1 mmol N/m^3 in ION and NWM. Accordingly, the mean bias and RMSD values also vary widely between subbasins and are highest in ADN for both FullDA and OpenDA. The sign of nitrate bias is both positive and negative in the OpenDA simulation, while it is negative in all of the subbasins and seasons in FullDA. ADS, ION and NWM show decreases in their absolute values of bias and concomitant decreases in their RMSD values. Only ADN shows that in shelf-seas an assimilation-induced decrease of nitrate triggers a worsening of the skill indexes in both seasons.

Since the assimilation scheme does not update nitrate, the decrease of nitrate concentration occurs during the model integration after the assimilation steps. According to the formulation of $\mathbf{V}_b$ (Teruzzi et al., 2014), when positive increments of chlorophyll are applied by DA, the phytoplankton internal content of carbon is updated proportionally, while the internal content of nitrate is increased of the amount necessary to keep the internal phytoplankton N:C ratio equal to the optimal value (set in BFM as equal to the Redfield ratio). Thus, if the N-content before the assimilation is high enough to have an N:C ratio greater than optimal even after the carbon increment, the phytoplankton internal content of nitrogen is not modified by the assimilation. This feature has been implemented to prevent the generation of too much mass of the

Table 5
Mean values of in situ data, RMSD and bias between FullDA and OpenDA and model in situ data (<0.01 indicates a negligible value ranging from −0.01 to 0.01; unavailable data are indicated with “-“).

Sub-basin	Bias win-spr		sum-aut		RMSD win-spr		sum-aut		Mean in situ	
	FullDA	OpenDA	FullDA	OpenDA	FullDA	OpenDA	FullDA	OpenDA	win-spr	sum-aut
Chlorophyll [mg chl/m^3]										
ADN	−1.06	−1.53	−0.64	−1.04	1.94	2.21	1.21	1.36	1.88	1.29
ADS	0.06	−0.08	0.05	−0.16	0.27	0.29	0.33	0.36	0.26	0.27
ION	–	–	−0.01	−0.01	–	–	0.05	0.05	–	0.09
TYR	−0.20	−0.25	−0.02	−0.03	0.25	0.30	0.04	0.04	0.39	0.07
Nitrate [mmol N/m^3]										
ADN	−13.63	−10.79	−5.47	−1.89	29.38	28.40	15.68	15.15	26.33	11.33
ADS	−0.32	0.41	−0.38	1.09	0.83	1.12	0.89	1.49	1.39	1.03
ION	−0.01	<0.01	–	–	0.67	0.66	–	–	0.80	–
NWM	−0.03	0.17	–	–	0.59	0.67	–	–	0.64	–
Phosphate [mmol P/m^3]										
ADN	−0.09	−0.08	−0.07	−0.09	0.19	0.19	0.16	0.17	0.16	0.15
NWM	0.01	0.01	<0.01	0.01	0.02	0.02	0.01	0.01	0.01	0.01

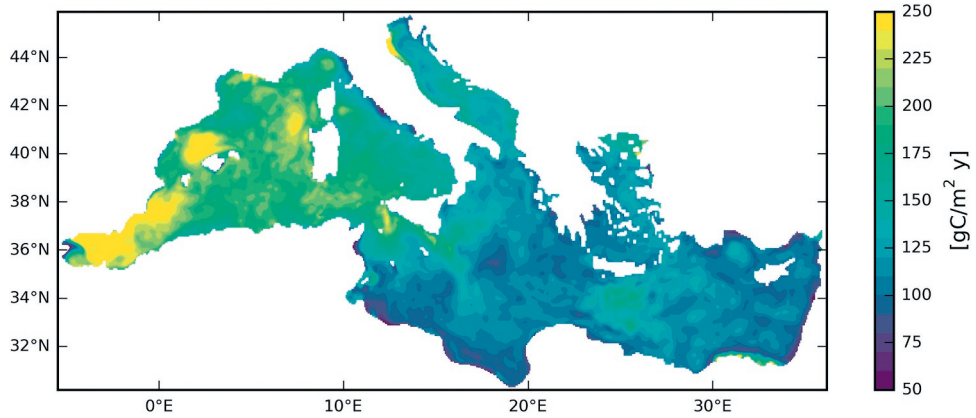

Fig. 7. Mean annual primary production integrated over 0–200 m in the year of simulation (2013).

non-limiting nutrient, which accumulate in phytoplankton according to the luxury uptake formulation of BFM (Vichi et al., 2015).

In the case of ADN, the phytoplankton N:C ratio before the assimilation is higher than the optimal value, and the assimilation scheme applies positive increments for chlorophyll. After the assimilation, the phytoplankton biomass is increased, and the N:C ratio is between the optimal and the maximum ratio allowed by the luxury-uptake of the non-limiting nutrient of the BFM parameterization (twice the Redfield ratio). The combination of (1) high availability of nitrate in ADN, (2) increased phytoplankton biomass and (3) lower-than-maximum phytoplankton N:C ratio causes an additional phytoplankton uptake of nitrate, that results in a reduction of nitrate concentration in sea water. It is worth to highlight that in our application the reduction of nitrate concentration in the Adriatic does not produce nitrate-limitation conditions, since the N:C ratio is always between the optimal and maximum value. On the other hand, phytoplankton growth is still phosphate-limited, as confirmed by an internal phytoplankton P:C ratio lower than the optimal value (in BFM equal to the Redfield ratio) and the N:P ratio in sea water higher than 16 molN/molP (Redfield; Lazzari et al., 2016).

3.3. Primary production

FullDA showed to improve the simulation of chlorophyll, thus based on the results of the FullDA simulation, we provide estimates of the vertically integrated mean annual primary production in the Mediterranean Sea shelf and open seas (Fig. 7). Although these results are based on a one-year simulation, they represent an upgrade of the basin-wide estimates discussed in Lazzari et al. (2012). These results are consistent with previous estimates from satellite observations (Bosc et al., 2004; Siokou-Frangou et al., 2010; Uitz et al., 2012), which showed that the western Mediterranean is more productive than the eastern Mediterranean: the mean primary production values in the eastern (ADN, ADS, AEG, ION and LEV) and western (ALB, SWW, SWE, NWM and TYR) subbasins are 117 gC/m^2/y and 188 gC/m^2/y, respectively. These values are higher than those provided by Lazzari et al. (2012) but in the range of other estimates of primary production in Mediterranean Sea at basin or sub-basin scale (Bosc et al., 2004; Bricaud et al., 2002; Kessouri et al., 2018; Siokou-Frangou et al., 2010; Uitz et al., 2012) with a mean primary production of 142 gC/m^2/y for the whole Mediterranean Sea for FullDA, which is 6% higher than in OpenDA.

Local patches of high production are depicted in Fig. 7, which highlights the heterogeneous presence of high-productivity areas close to the coasts (i.e., the western part of the Italian Adriatic coast, Dardanelles and Nile mouth regions) that are not shown in Lazzari et al. (2012). In the eastern Mediterranean, the presence of shelf areas with high productivity indicates that the mean integrated primary production is higher in shelf seas than it is in the open sea. For instance, in the Adriatic Sea, the mean values of primary production are 143 gC/m^2/y and 133 gC/m^2/y in shelf and open sea, respectively. In contrast, in the western Mediterranean, the mean primary production is higher in the open sea (with a mean value of 191 gC/m^2/y, compared with that of 168 gC/m^2/y in shelf seas), thus highlighting that in the Western Mediterranean shelf-seas phenomena are not so relevant to primary production as in the Adriatic Sea, which is a semi-enclosed basin strongly affected by coastal processes. Similar results have been obtained in a study focused on the fertilization sources in the Mediterranean Sea (Macias. et al., 2017). The results obtained using FullDA indicate that the model reproduces the relevant spatial variability of primary production, and highlight the prominent role that shelf-seas play in primary production in some specific areas of the Mediterranean Sea, which is an aspect difficult to capture using only in situ measurements.

4. Discussion

In the present study, we showed how case 2 water remote chlorophyll observations can be efficiently integrated in a complex biogeochemical model using a 3DVAR data assimilation scheme to better describe the phytoplankton dynamics and their spatial patterns in the Mediterranean shelf seas. The modelled results have been validated against independent in situ observations of chlorophyll and nutrients along the Italian coast (validation for open sea areas is provided in Teruzzi et al., 2014). The results of comparisons with independent in situ observations are encouraging. Indeed, the FullDA simulation substantially improves the statistics of the assimilated variable (chlorophyll) in all of the subbasins while slightly improving or at least not deteriorating the skill statistics of nutrients, except for nitrate in the northern Adriatic.

The statistics evaluated for chlorophyll and nutrients are comparable to those provided in Fraysse et al. (2013) in an area of the northwestern Mediterranean, as the root mean square difference (RMSD) between in situ observations and model values is the same order of magnitude as the mean in situ measurements. In a recent application of biogeochemical assimilation in the Mediterranean Sea (Tsiaras et al., 2017), the RMSD values obtained from the comparison with a climatology based on in situ data are similar to those obtained in the present study for phosphate, while the RMSD values of nitrate are significantly lower in the present study. The results of the validation are even more interesting when considering that most of the in situ data have been collected at very shallow locations (i.e., in the first model grid-point from the coastline), and they thus describe very local and near-shore dynamics that are not properly simulated by the model itself.

The decrease of nitrate concentration in the northern Adriatic, which deteriorates the skill statistics in this area, is due to a

combination of the $\mathbf{V}_b$ operator (which produces higher phytoplankton biomasses with a reduced internal N:C ratio in this particular case) and the luxury uptake mechanism for a non-limiting nutrient of the BFM model (Lazzari et al., 2016). This condition increases the phytoplankton uptake of nitrate and consequently its concentration decreases. An improvement of the representation of non-assimilated variables is not straightforward in biogeochemical DA for state estimation as shown in previous publications: as an example, Ford et al. (2012) indicate as a good result of their assimilation the non-degradation of non-assimilated variables. Other works clearly indicate and comment on degradation of some non-assimilated variables, especially nutrients (Ciavatta et al., 2014; Fontana et al., 2013; Ford et al., 2012; Shulman et al., 2013; Simon et al., 2015; Tsiaras et al., 2017). Our results highlight the complexity of the biogeochemical response to data assimilation and the need to investigate the specific response of non-assimilated variables in biogeochemical models.

Further improvements on nutrients could be obtained by the implementation of a multivariate $\mathbf{V}_b$ operator accounting for the covariance between chlorophyll and nutrients. In complex biogeochemical models, such as OGSTM-BFM, the definition of a thorough covariance between chlorophyll and nutrients is not a trivial task. Indeed, the relationship between phytoplankton chlorophyll and external nutrients is not linear nor constant in time and space, and regulated by different processes: chlorophyll synthesis, phytoplankton growth phase, and nutrient uptake. The definition of a covariance $\mathbf{V}_b$ operator could be realised using two different approaches: an error covariance matrix built on long term model simulations (e.g., Shulman et al., 2013) or on the spreading of an ensemble (e.g., Ciavatta et al., 2014; Tsiaras et al., 2017); a dynamical inverse model, similarly to the compensation model proposed by Hemmings et al. (2008).

The persistence of the DA updates in the shelf seas is of the order of five days (Fig. 5). The relative low persistence is mainly due to the phytoplankton photoadaptation mechanism and to the decoupled phytoplankton growth and nutrient uptake. In the BFM phytoplankton formulation, the growth and the nutrient uptake are two decoupled phases: the nutrients uptake is related to the external nutrient availability and to the distance from a phytoplankton optimal nutrient internal quota, while the growth-lysis is related, besides other factors, to the phytoplankton nutrient internal quota (details in Lazzari et al., 2012). All these peculiar aspects of the BFM formulation point out the need for a more elaborated $\mathbf{V}_b$ operator, involving either a different response of the chlorophyll synthesis to the actual light conditions or the update of the external nutrient concentrations, which contribute to regulate the growth rate and chlorophyll synthesis through the uptake mechanism.

Mass conservation is not a constraint that is generally respected by the formulation of the covariance between the biogeochemical variables in state-estimation assimilation schemes. Few examples of biogeochemical DA for state estimation with mass conservation have been presented in literature (e.g., the method of Hemmings et al., 2008 and its applications in Ford et al., 2012). On the contrary, several recent applications in realistic framework of biogeochemical DA for state estimation do not include a mass-conservation constraint (Ciavatta et al., 2014, 2016; Fontana et al., 2010, 2013; Hu et al., 2012; Jones et al., 2016; Shulman et al., 2013; Simon et al., 2015; Song et al., 2016a; Tsiaras et al., 2017). In some of these works the mass conservation issue is explicitly discussed. In Ciavatta et al. (2014) the absence of a mass conservation constraint in sequential assimilation is ascribed to the uncertainty of mass balance inherently present in biogeochemical models. Hu et al. (2012) evaluate the impact of DA on the total mass of nitrogen, while Song et al. (2016a) compare the increments introduced at each assimilation cycle with other system fluxes.

A mass conservation constraint is not included in our data assimilation, and we evaluated the additional terms to the system budget due to DA for nitrogen (since nitrate is the variable mostly affected by the assimilation). The sum of these terms in FullDA simulation equals to less than 1% of the Mediterranean annual primary production (in nitrogen unit) and to 17% of the annual input of nitrogen from atmosphere and rivers. Given an uncertainty of more than 100% in atmospheric input (D'Ortenzio and Ribera d' Alcala et al. 2009) and the many possible sources of uncertainty in river estimates (Ludwig et al., 2010), the lack of mass conservation appears not relevant.

The full-basin assimilation of satellite chlorophyll observations allows for several improvements in the simulation of phytoplankton in the Mediterranean shelf seas. These improvements cannot be otherwise obtained by a biogeochemical model whose formulation and setup are optimised for the representation of open sea dynamics (Cossarini et al., 2015; Lazzari et al., 2012). In particular, because of the use of climatological boundary conditions (especially at rivers), the relatively low resolution of the model (i.e., fertilization effects due to minor terrestrial inputs are not considered in the basin-wide simulation) and the lack of interaction between the water column and the bottom (the BFM model does not include a benthic component).

Shelf seas are characterised by chlorophyll concentration patterns with high spatial and temporal variability induced by several coastal processes (e.g., riverine inputs, local vertical mixing events due to the interactions between currents and morphology; Mann and Lazier, 2005). Data assimilation might be particularly relevant to address these additional sources of uncertainties. In particular, coastal-water DA should be able to propagate the updates in agreement with the dynamic properties of the current field. In other words, the entity and major directions of propagation of the DA updates should adapt to the current-field changes (that can be also due to changes in riverine inputs). Our methodology provide a steps toward this direction. Consistent with this framework, the present shelf-seas data assimilation scheme reproduces a more reliable description of the higher chlorophyll values close to the river mouths also increasing the spatial variability of chlorophyll concentration in shelf seas.

A reliable description of the phenomena related to riverine inputs is usually intrinsically limited in basin-wide biogeochemical models that use riverine nutrient discharge based on climatological references (such as the implementation of the BFM in the Mediterranean Sea and its present configuration adopted in CMEMS). Considering the difficulties associated with designing and maintaining a monitoring plan for river nutrient discharge or creating reliable and validated datasets of river discharge at high spatial and temporal resolution (Ludwig et al., 2009), or even those associated with coupling a biogeochemical model to a hydrological one to estimate nutrient loads, the assimilation of satellite observations may provide an alternative and efficient method of integrating riverine effects into a model simulation. Thus, the implementation of DA of shelf-seas data in a multiannual simulation (e.g., reanalysis) can compensate for the use of climatological riverine nutrient discharge taking in account inter-annual variability of chlorophyll concentration.

Defining the background covariance operators in shelf seas should account for the specificity of shelf-seas processes in both the vertical and horizontal dimensions. In shelf seas, vertical chlorophyll dynamics are not directly dominated by the seasonal cycle of surface winter bloom and summer stratification that are typical of the open sea. Furthermore, we showed that in shelf seas, the horizontal variability increases by nearly 30% (in terms of increase of the chlorophyll horizontal gradient, Table 4), thus indicating that morphological features can introduce strong anisotropy and affect relevant local dynamics. Accordingly, the background error covariance has been modified to update both the vertical and horizontal operators.

The horizontal error covariance has been designed using two non-uniform radii, L_x and L_y, for longitude and latitude, respectively, in shelf seas. The chlorophyll field produced using the assimilation scheme with the new horizontal operator better reproduces the values and spatial distribution of satellite chlorophyll in shelf seas. Non-uniform and anisotropic correlation length scales have previously been proposed for 3DVAR assimilation in a global ocean circulation model, and the

benefits of this approach have been highlighted especially in eddy-dominated areas and tropical areas where the longitudinal and latitudinal correlation length scales are significantly different (Storto et al., 2014). In an operational framework, a method for the evaluation of non-uniform correlation radii based on the surface salinity gradient can be implemented using the salinity fields operationally obtained using a general circulation model forecasting system, thus adapting the horizontal error covariance operator to the driving hydrodynamic field. However, this method will also result in a not-negligible increase in the computational costs associated with the operational implementation of the assimilation scheme.

The new vertical operator is based on a finer subdivision of the shelf seas obtained using a *k*-means analysis. This subdivision distinguishes shelf areas affected by river runoff from areas located far from the influence of terrestrial forcing. Grid-point-dependent vertical correlation could also be used to identify local vertical dynamics. In the present case, we chose to use a subbasin subdivision approach to limit the computational costs of the vertical EOF evaluation, and we applied two smoothing factors to avoid sharp variations in the vertical operators between the subbasins. First, the tuning of the EOF eigenvalue based on the relationship between the observation error and innovation at the grid-point-level guarantees that the EOFs are not strictly uniform in each subbasin. Second, the application of $\mathbf{V}_h$ after the $\mathbf{V}_v$ operator provides an additional smoothing effect, as was shown by Dobricic and Pinardi (2008).

The covariance of observation errors is crucial when dealing with shelf-seas assimilation in order to guarantee the effective integration of satellite observations. It has been highlighted that the definition of observation uncertainties provided by the error covariance matrix is relevant to the assimilation of satellite chlorophyll (Dowd et al., 2014). In the present work, we assumed that the observation error is proportional to the field variance. A similar approach has been adopted in Shulman et al. (2013), where the representation error was estimated as proportional to the variance of the observations. Given the high variability of surface chlorophyll concentration in coastal water, this approach would imply higher error in coastal waters, where relevant temporal variability occurs. As a pragmatic approach, we imposed a maximum ratio between the observation and background error to guarantee an effective assimilation of satellite observations.

This approach has been adopted considering that the evaluation of the observation errors is not uniquely defined. Dowd et al. (2014) noted that the algorithm used for the evaluation of chlorophyll concentration should be approached as a model with its own accuracy errors, which should be considered in data assimilation schemes. An example of the estimation of related background and observation error covariance matrices for satellite chlorophyll is presented in Ford and Barciela (2017). Alternatively, some applications have demonstrated the feasibility of directly assimilating optical data from ocean colour (Ciavatta et al., 2014; Jones et al., 2016; Shulman et al., 2013), thus avoiding the evaluation of the chlorophyll algorithm-related error but, on the other hand, requiring the parameterization of the optical properties of water in the marine ecosystem model.

Several results of a biogeochemical model can benefit from a better description of phytoplankton chlorophyll. For example, based on the updated and validated representation of the shelf and open sea Mediterranean Sea chlorophyll, we provide an estimate of the phytoplankton primary production. These results update the former estimate presented in Lazzari et al. (2012) and show that primary production in the western Mediterranean is mainly located in the open sea, whilst in the eastern Mediterranean, the areas with the highest primary production are mostly located in shelf seas. This difference indicates that primary production is mainly related to nutrient flow due to open-sea vertical convection in the western Mediterranean (Lavigne et al., 2013; Lazzari et al., 2012, 2016; Taylor and Ferrari, 2011) and riverine inputs (i.e., coastal processes) in the eastern Mediterranean.

As a final consideration, we highlight that dealing with both shelf and open sea data means significantly increasing the range of the variability of observations (i.e., chlorophyll concentration values can range over more than two orders of magnitude). Thus, the observed distribution might be quite far from the Gaussian distribution; in this case, previous studies have proposed the use of the log-transformation (Ford and Barciela, 2017; Song et al., 2016b), as well as anamorphic transformations (Doron et al., 2013) or particle filtering (Mattern et al., 2013). In the present study, we used the natural values of chlorophyll concentration because using log-normal values might result in a non-optimal solution of the cost function, as discussed in Teruzzi et al. (2014). Moreover, the non-log-transformed space is more representative of the vertical dynamics of the vertical operator of background error decomposition, and it thus preserves the typical shapes of the modelled chlorophyll profiles observed in the Mediterranean Sea.

5. Conclusions

We developed and applied a three-dimensional variational scheme for the assimilation of satellite chlorophyll observations in coastal waters, in order to assimilate both open-sea and shelf-sea data. The data assimilation scheme for coastal waters features a non-homogenous vertical component and a non-uniform and direction-dependent horizontal component of the background error covariance. The results show that the data assimilation updates are propagated consistently to the salinity gradient field, i.e., a dynamic property that tracks currents and river inputs, providing an improved simulation of the spatial variability and seasonal cycle of chlorophyll concentration in Mediterranean coastal waters. The use of shelf-seas satellite observations of chlorophyll demonstrates the potentiality to improve the quality of the CMEMS operational biogeochemical products in the Mediterranean Sea, although further research is still needed to improve the forecast also for non-assimilated variables.

Acknowledgements

We acknowledge V. Bandelj from OGS and A. Bruschi from ISPRA for the support in the processing of the in situ data used for the validation, and the Reviewers for their valuable comments that helped us to improve the quality of this work.

We acknowledge the CINECA award under the ISCRA initiative (MEDCOAST), for the availability of high performance computing resources and support.

This study has been conducted using E.U. Copernicus Marine Service Information.

Appendix A. Definition of shelf-seas *k*-regions through a *k*-means analysis

The $\mathbf{V}_v$ operator in the shelf Mediterranean seas has been constructed introducing a finer spatial subdivision compared to the one proposed for the open sea in Teruzzi et al. (2014). A *k*-means analysis has been applied to subdivide each of the 10 regions identified in Lazzari et al. (2012) in the shelf-seas. The *k*-means analysis aims to partition a set of data $\mathbf{x}$ into a predefined number k of clusters such that each data belongs to the cluster with the nearest mean (MacQueen, 1967). Operatively, the *k*-means analysis provides a set of objects $[\boldsymbol{U}_1, \ldots, \boldsymbol{U}_k]$ into which each element of the data set $\mathbf{x}$ is classified, minimizing the sum of the distance of the elements of the data set from the centroid of the cluster:

$$min\left(\sum_{i=1}^{k}\sum_{x\in U_i}||\boldsymbol{x}-\boldsymbol{C}_i||\right), \tag{A1}$$

where $\boldsymbol{x}\in\boldsymbol{U_i}$ are the elements of the data set that are classified into each cluster $\boldsymbol{U}_i$, while $\boldsymbol{C}_i$ are the centroids of the clusters $\boldsymbol{U}_i$ (defined as the mean of the elements $\boldsymbol{x}\in\boldsymbol{U_i}$). In our application the elements of the dataset are the mean monthly chlorophyll profiles for all the shelf-seas points of a given Mediterranean subbasin. Thus, the dimension of an element of $\boldsymbol{x}$ and of the centroids are equal to 12 (number of months) times the number of chlorophyll profile levels. The mean chlorophyll profiles are computed as climatological average from the 1999–2015 CMEMS reanalysis (Teruzzi et al., 2016).

The Euclidean distance has been applied for the evaluation of the norm $\|\|$ in Eq. (A1). An iterative refinement algorithm (available in the Scipy Python Package) has been used for the minimization of Eq. (A1). The analysis has been repeated twice using a random initialisation at the first step, and the results of the first step as initialisation for the second one. For each subbasin, the analysis has been repeated using a number of clusters k ranging from two to five. Considering the high spatial patchiness of the clusters obtained with higher values of k, the number of clusters k has been pragmatically chosen equal to two for all the subbasins.

References

Arin, L., Guillén, J., Segura-Noguera, M., Estrada, M., 2013. Open sea hydrographic forcing of nutrient and phytoplankton dynamics in a Mediterranean coastal ecosystem. Estuar. Coast. Shelf Sci. 133, 116–128. https://doi.org/10.1016/j.ecss.2013.08.018.

Arruda, R., Calil, P.H.R., Bianchi, A.A., Doney, S.C., Gruber, N., Lima, I., Turi, G., 2015. Air-sea CO_2 fluxes and the controls on ocean surface pCO_2 seasonal variability in the coastal and open-ocean southwestern Atlantic Ocean: a modeling study. Biogeosciences 12, 5793–5809. https://doi.org/10.5194/bg-12-5793-2015.

Beltrán-Abaunza, J.M., Kratzer, S., Höglander, H., 2017. Using MERIS data to assess the spatial and temporal variability of phytoplankton in coastal areas. Int. J. Remote Sens. 38, 2004–2028. https://doi.org/10.1080/01431161.2016.1249307.

Béthoux, J.P., Morin, P., Chaumery, C., Connan, O., Gentili, B., Ruiz-Pino, D., 1998. Nutrients in the Mediterranean Sea, mass balance and statistical analysis of concentrations with respect to environmental change. Mar. Chem. 63, 155–169. https://doi.org/10.1016/S0304-4203(98)00059-0.

Blondeau-Patissier, D., Schroeder, T., Brando, V.E., Maier, S.W., Dekker, A.G., Phinn, S., 2014. ESA-MERIS 10-year mission reveals contrasting phytoplankton bloom dynamics in two tropical regions of Northern Australia. Remote Sens. 6, 2963–2988. https://doi.org/10.3390/rs6042963.

Bolzon, G., Cossarini, G., Lazzari, P., Salon, S., Teruzzi, A., Crise, A., Solidoro, C., 2017. Mediterranean Sea biogeochemical analysis and forecast (CMEMS MED AF-biogeochemistry 2013–2017). https://doi.org/10.25423/MEDSEA_ANALYSIS_FORECAST_BIO_006_006.

Bolzon, G., Cossarini, G., Lazzari, P., Salon, S., Teruzzi, A., Crise, A., Solidoro, C., 2018. Mediterranean Sea biogeochemical analysis and forecast (CMEMS MED-biogeochemistry 2015–2018). https://doi.org/10.25423/CMCC/MEDSEA_ANALYSIS_FORECAST_BIO_006_014.

Bosc, E., Bricaud, A., Antoine, D., 2004. Seasonal and interannual variability in algal biomass and primary production in the Mediterranean Sea, as derived from 4 years of SeaWiFS observations. Glob. Biogeochem. Cycles 18, GB1005. https://doi.org/10.1029/2003GB002034.

Bricaud, A., Bosc, E., Antoine, D., 2002. Algal biomass and sea surface temperature in the Mediterranean basin: intercomparison of data from various satellite sensors, and implications for primary production estimates. Remote Sens. Environ. 81, 163–178. https://doi.org/10.1016/S0034-4257(01)00335-2.

Campbell, R., Diaz, F., Hu, Z., Doglioli, A., Petrenko, A., Dekeyser, I., 2013. Nutrients and plankton spatial distributions induced by a coastal eddy in the Gulf of Lion. Insights Numer. Model. Prog. Oceanogr. 109, 47–69. https://doi.org/10.1016/j.pocean.2012.09.005.

Carvalho, G.A., Minnett, P.J., Banzon, V.F., Baringer, W., Heil, C.A., 2011. Long-term evaluation of three satellite ocean color algorithms for identifying harmful algal blooms (Karenia brevis) along the west coast of Florida: a matchup assessment. Remote Sens. Environ. 115, 1–18. https://doi.org/10.1016/j.rse.2010.07.007.

Ciavatta, S., Kay, S., Saux-Picart, S., Butenschön, M., Allen, J.I., 2016. Decadal reanalysis of biogeochemical indicators and fluxes in the North West European shelf-sea ecosystem. J. Geophys. Res. Oceans 121, 1824–1845. https://doi.org/10.1002/2015JC011496.

Ciavatta, S., Torres, R., Martinez-Vicente, V., Smyth, T., Dall'Olmo, G., Polimene, L., Allen, J.I., 2014. Assimilation of remotely-sensed optical properties to improve marine biogeochemistry modelling. Prog. Oceanogr. 127, 74–95. https://doi.org/10.1016/j.pocean.2014.06.002.

Colella, S., Falcini, F., Rinaldi, E., Sammartino, M., Santoleri, R., 2016. Mediterranean Ocean colour chlorophyll trends. PLoS One 11, e0155756. https://doi.org/10.1371/journal.pone.0155756.

Cossarini, G., Lermusiaux, P.F.J., Solidoro, C., 2009. Lagoon of Venice ecosystem: seasonal dynamics and environmental guidance with uncertainty analyses and error subspace data assimilation. J. Geophys. Res. Oceans 114, C06026. https://doi.org/10.1029/2008JC005080.

Cossarini, G., Querin, S., Solidoro, C., 2015. The continental shelf carbon pump in the northern Adriatic Sea (Mediterranean Sea): Influence of wintertime variability. Ecol. Model. 314, 118–134. https://doi.org/10.1016/j.ecolmodel.2015.07.024.

Cossarini, G., Solidoro, C., 2008. Global sensitivity analysis of a trophodynamic model of the Gulf of Trieste. Ecol. Model. In: Selected Papers from the Fifth European Conference on Ecological Modelling, 19–23 September 2005. Pushchino, Russia. 212. pp. 16–27. https://doi.org/10.1016/j.ecolmodel.2007.10.009.

Cossarini, G., Solidoro, C., Fonda Umani, S., 2012. Dynamics of biogeochemical properties in temperate coastal areas of freshwater influence: lessons from the Northern Adriatic Sea (Gulf of Trieste). Fluctuations and trends in the northern Adriatic marine systems: from annual to decadal variability. Estuar. Coast. Shelf Sci. 115, 63–74. https://doi.org/10.1016/j.ecss.2012.02.006.

Crise, A., Allen, J.I., Baretta, J., Crispi, G., Mosetti, R., Solidoro, C., 1999. The Mediterranean pelagic ecosystem response to physical forcing. Prog. Oceanogr. 44, 219–243. https://doi.org/10.1016/S0079-6611(99)00027-0.

Da, F., Friedrichs, M.A.M., St-Laurent, P., 2018. Impacts of atmospheric nitrogen deposition and coastal nitrogen fluxes on oxygen concentrations in Chesapeake Bay. J. Geophys. Res. Oceans 123, 5004–5025. https://doi.org/10.1029/2018JC014009.

D'Alimonte, D., Melin, F., Zibordi, G., Berthon, J.F., 2003. Use of the novelty detection technique to identify the range of applicability of empirical ocean color algorithms. IEEE Trans. Geosci. Remote Sens. 41, 2833–2843. https://doi.org/10.1109/TGRS.2003.818020.

D'Alimonte, D., Zibordi, G., 2003. Phytoplankton determination in an optically complex coastal region using a multilayer perceptron neural network. IEEE Trans. Geosci. Remote Sens. 41, 2861–2868. https://doi.org/10.1109/TGRS.2003.817682.

Denman, K.L., Powell, T.M., 1984. Effects of physical processes on planktonic ecosystems in the coastal ocean. Oceangr. Mar. Biol. Annu. Rev. 22, 125–168.

Desroziers, G., Berre, L., Chapnik, B., Poli, P., 2005. Diagnosis of observation, background and analysis-error statistics in observation space. Q. J. R. Meteorol. Soc. 131, 3385–3396. https://doi.org/10.1256/qj.05.108.

Dobricic, S., Pinardi, N., 2008. An oceanographic three-dimensional variational data assimilation scheme. Ocean Model. 22, 89–105. https://doi.org/10.1016/j.ocemod.2008.01.004.

Doron, M., Brasseur, P., Brankart, J.-M., Losa, S.N., Melet, A., 2013. Stochastic estimation of biogeochemical parameters from Globcolour ocean colour satellite data in a North Atlantic 3D ocean coupled physical–biogeochemical model. J. Mar. Syst. 117–118, 81–95. https://doi.org/10.1016/j.jmarsys.2013.02.007.

D'Ortenzio, F., Ribera d'Alcalà, M, 2009. On the trophic regimes of the Mediterranean Sea: a satellite analysis. Biogeosciences 6, 139–148. https://doi.org/10.5194/bg-6-139-2009.

Dowd, M., Jones, E., Parslow, J., 2014. A statistical overview and perspectives on data assimilation for marine biogeochemical models. Environmetrics 25, 203–213. https://doi.org/10.1002/env.2264.

Edwards, C.A., Moore, A.M., Hoteit, I., Cornuelle, B.D., 2015. Regional Ocean Data Assimilation. Ann. Rev. Mar. Sci. 7, 21–42. https://doi.org/10.1146/annurev-marine-010814-015821.

Ennet, P., Kuosa, H., Tamsalu, R., 2000. The influence of upwelling and entrainment on the algal bloom in the Baltic Sea. J. Mar. Syst. 25, 359–367. https://doi.org/10.1016/S0924-7963(00)00027-0.

Fontana, C., Brasseur, P., Brankart, J.-M., 2013. Toward a multivariate reanalysis of the North Atlantic Ocean biogeochemistry during 1998–2006 based on the assimilation of SeaWiFS chlorophyll data. Ocean Sci. 9, 37–56. https://doi.org/10.5194/os-9-37-2013.

Fontana, C., Grenz, C., Pinazo, C., 2010. Sequential assimilation of a year-long time-series of SeaWiFS chlorophyll data into a 3D biogeochemical model on the French Mediterranean coast. Cont. Shelf Res. 30, 1761–1771. https://doi.org/10.1016/j.csr.2010.08.003.

Fontana, C., Grenz, C., Pinazo, C., Marsaleix, P., Diaz, F., 2009. Assimilation of SeaWiFS chlorophyll data into a 3D-coupled physical–biogeochemical model applied to a freshwater-influenced coastal zone. Cont. Shelf Res. 29, 1397–1409. https://doi.org/10.1016/j.csr.2009.03.005.

Ford, D., Barciela, R., 2017. Global marine biogeochemical reanalyses assimilating two different sets of merged ocean colour products. Earth Observation of Essential Climate Variables. Remote Sens. Environ. 203, 40–54. https://doi.org/10.1016/j.rse.2017.03.040.

Ford, D.A., Edwards, K.P., Lea, D., Barciela, R.M., Martin, M.J., Demaria, J., 2012. Assimilating GlobColour ocean colour data into a pre-operational physical-biogeochemical model. Ocean Sci. 8, 751–771. https://doi.org/10.5194/os-8-751-2012.

Foujols, M.-A., Lévy, M., Aumont, O., Madec, G., 2000. OPA 8.1 Tracer Model Reference

Manual. Institut Pierre Simon Laplace, pp. 39.
Fraysse, M., Pinazo, C., Faure, V.M., Fuchs, R., Lazzari, P., Raimbault, P., Pairaud, I., 2013. Development of a 3D coupled physical-biogeochemical model for the Marseille coastal area (NW Mediterranean Sea): what complexity is required in the coastal zone? PLoS One 8, e80012. https://doi.org/10.1371/journal.pone.0080012.
Friedrichs, M.A.M., Hofmann, E.E., 2001. Physical control of biological processes in the central equatorial Pacific Ocean. Deep Sea Res. Part I 48, 1023–1069. https://doi.org/10.1016/S0967-0637(00)00079-0.
Gaetan, C., Girardi, P., Pastres, R., Mangin, A., 2016. Clustering chlorophyll-a satellite data using quantiles. Ann. Appl. Stat. 10, 964–988. https://doi.org/10.1214/16-AOAS923.
Gazeau, F., Smith, S.V., Gentili, B., Frankignoulle, M., Gattuso, J.-P., 2004. The European coastal zone: characterization and first assessment of ecosystem metabolism. Estuar. Coast. Shelf Sci. 60, 673–694. https://doi.org/10.1016/j.ecss.2004.03.007.
Giani, M., Djakovac, T., Degobbis, D., Cozzi, S., Solidoro, C., Umani, S.F., 2012. Recent changes in the marine ecosystems of the northern Adriatic Sea. Fluctuations and trends in the northern Adriatic marine systems: from annual to decadal variability. Estuar. Coast. Shelf Sci. 115, 1–13. https://doi.org/10.1016/j.ecss.2012.08.023.
Gohin, F., Saulquin, B., Oger-Jeanneret, H., Lozac'h, L., Lampert, L., Lefebvre, A., Riou, P., Bruchon, F., 2008. Towards a better assessment of the ecological status of coastal waters using satellite-derived chlorophyll-a concentrations. Earth observations for marine and coastal biodiversity and ecosystems special issue. Remote Sens. Environ. 112, 3329–3340. https://doi.org/10.1016/j.rse.2008.02.014.
Guadayol, Ò., Peters, F., Marrasé, C., Gasol, J., Roldán, C., Berdalet, E., Massana, R., Sabata, A., 2009. Episodic meteorological and nutrient-load events as drivers of coastal planktonic ecosystem dynamics: a time-series analysis. Mar. Ecol. Prog. Ser. 381, 139–155. https://doi.org/10.3354/meps07939.
Harding, L.W., Gallegos, C.L., Perry, E.S., Miller, W.D., Adolf, J.E., Mallonee, M.E., Paerl, H.W., 2016. Long-term trends of nutrients and phytoplankton in Chesapeake Bay. Estuar. Coasts 39, 664–681. https://doi.org/10.1007/s12237-015-0023-7.
Harvey, E.T., Kratzer, S., Philipson, P., 2015. Satellite-based water quality monitoring for improved spatial and temporal retrieval of chlorophyll-a in coastal waters. Remote Sens. Environ. 158, 417–430. https://doi.org/10.1016/j.rse.2014.11.017.
Hemmings, J.C.P., Barciela, R.M., Bell, M.J., 2008. Ocean color data assimilation with material conservation for improving model estimates of air-sea CO_2 flux. J. Mar. Res. 66, 87–126. https://doi.org/10.1357/002224008784815739.
Hofmann, E.E., Cahill, B., Fennel, K., Friedrichs, M.A.M., Hyde, K., Lee, C., Mannino, A., Najjar, R.G., O'Reilly, J.E., Wilkin, J., Xue, J., 2011. Modeling the dynamics of continental shelf carbon. Annu. Rev. Mar. Sci. 3, 93–122. https://doi.org/10.1146/annurev-marine-120709-142740.
Holt, J., Butenschön, M., Wakelin, S.L., Artioli, Y., Allen, J.I., 2012. Oceanic controls on the primary production of the northwest European continental shelf: model experiments under recent past conditions and a potential future scenario. Biogeosciences 9, 97–117. https://doi.org/10.5194/bg-9-97-2012.
Hu, J., Fennel, K., Mattern, J.P., Wilkin, J., 2012. Data assimilation with a local ensemble Kalman filter applied to a three-dimensional biological model of the Middle Atlantic Bight. J. Mar. Syst. 94, 145–156. https://doi.org/10.1016/j.jmarsys.2011.11.016.
Jones, E.M., Baird, M.E., Mongin, M., Parslow, J., Skerratt, J., Lovell, J., Margvelashvili, N., Matear, R.J., Wild-Allen, K., Robson, B., Rizwi, F., Oke, P., King, E., Schroeder, T., Steven, A., Taylor, J., 2016. Use of remote-sensing reflectance to constrain a data assimilating marine biogeochemical model of the Great Barrier Reef. Biogeosciences 13, 6441–6469. https://doi.org/10.5194/bg-13-6441-2016.
Kalaroni, S., Tsiaras, K., Petihakis, G., Hoteit, I., Economou-Amilli, A., Triantafyllou, G., 2016. Data assimilation of depth-distributed satellite chlorophyll-α in two Mediterranean contrasting sites. J. Mar. Syst. 160, 40–53. https://doi.org/10.1016/j.jmarsys.2016.03.018.
Kessouri, F., Ulses, C., Estournel, C., Marsaleix, P., D'Ortenzio, F., Severin, T., Taillandier, V., Conan, P., 2018. Vertical mixing effects on phytoplankton dynamics and organic carbon export in the western Mediterranean Sea. J. Geophys. Res. Oceans. https://doi.org/10.1002/2016JC012669@10.1002/(ISSN)2169-9291.DENSEWATER01.
Krom, M.D., Kress, N., Brenner, S., Gordon, L.I., 1991. Phosphorus limitation of primary productivity in the eastern Mediterranean Sea. Limnol. Oceanogr. 36, 424–432. https://doi.org/10.4319/lo.1991.36.3.0424.
Kuosa, H., Fleming-Lehtinen, V., Lehtinen, S., Lehtiniemi, M., Nygård, H., Raateoja, M., Raitaniemi, J., Tuimala, J., Uusitalo, L., Suikkanen, S., 2017. A retrospective view of the development of the Gulf of Bothnia ecosystem. J. Mar. Syst. 167, 78–92. https://doi.org/10.1016/j.jmarsys.2016.11.020.
Lavigne, H., D'Ortenzio, F., Migon, C., Claustre, H., Testor, P., Ribera d'Alcalà, M., Lavezza, R., Houpert, L., Prieur, L., 2013. Enhancing the comprehension of mixed layer depth control on the Mediterranean phytoplankton phenology. J. Geophys. Res. Oceans 118, 3416–3430. https://doi:10.1002/jgrc.20251.
Lazzari, P., Solidoro, C., Ibello, V., Salon, S., Teruzzi, A., Béranger, K., Colella, S., Crise, A., 2012. Seasonal and inter-annual variability of plankton chlorophyll and primary production in the Mediterranean Sea: a modelling approach. Biogeosciences 9, 217–233. https://doi.org/10.5194/bg-9-217-2012.
Lazzari, P., Solidoro, C., Salon, S., Bolzon, G., 2016. Spatial variability of phosphate and nitrate in the Mediterranean Sea: a modeling approach. Deep Sea Res. Part I 108, 39–52. https://doi.org/10.1016/j.dsr.2015.12.006.
Lazzari, P., Teruzzi, A., Salon, S., Campagna, S., Calonaci, C., Colella, S., Tonani, M., Crise, A., 2010. Pre-operational short-term forecasts for Mediterranean Sea biogeochemistry. Ocean Sci. 6, 25–39. https://doi.org/10.5194/os-6-25-2010.
Le Traon, P.-Y., Antoine, D., Bentamy, A., Bonekamp, H., Breivik, L.A., Chapron, B., Corlett, G., Dibarboure, G., DiGiacomo, P., Donlon, C., Faugère, Y., Font, J., Girard-Ardhuin, F., Gohin, F., Johannessen, J.A., Kamachi, M., Lagerloef, G., Lambin, J., Larnicol, G., Borgne, P.L., Leuliette, E., Lindstrom, E., Martin, M.J., Maturi, E., Miller, L., Mingsen, L., Morrow, R., Reul, N., Rio, M.H., Roquet, H., Santoleri, R., Wilkin, J., 2015. Use of satellite observations for operational oceanography: recent achievements and future prospects. J. Oper. Oceanogr. 8, s12–s27. https://doi.org/10.1080/1755876X.2015.1022050.
Lionello, P. (Ed.), 2012. The Climate of the Mediterranean Region. Elsevier, Oxford, pp. i–iii. https://doi.org/10.1016/B978-0-12-416042-2.00009-4.
Loisel, H., Vantrepotte, V., Ouillon, S., Ngoc, D.D., Herrmann, M., Tran, V., Mériaux, X., Dessailly, D., Jamet, C., Duhaut, T., Nguyen, H.H., Van Nguyen, T., 2017. Assessment and analysis of the chlorophyll-a concentration variability over the Vietnamese coastal waters from the MERIS ocean color sensor (2002–2012). Remote Sens. Environ. 190, 217–232. https://doi.org/10.1016/j.rse.2016.12.016.
Ludwig, W., Bouwman, A.F., Dumont, E., Lespinas, F., 2010. Water and nutrient fluxes from major Mediterranean and Black Sea rivers: Past and future trends and their implications for the basin-scale budgets. Glob. Biogeochem. Cycles 24. https://doi.org/10.1029/2009GB003594.
Ludwig, W., Dumont, E., Meybeck, M., Heussner, S., 2009. River discharges of water and nutrients to the Mediterranean and Black Sea: major drivers for ecosystem changes during past and future decades? Prog. Oceanogr. 80, 199–217. https://doi.org/10.1016/j.pocean.2009.02.001.
Lynch, T.P., Morello, E.B., Evans, K., Richardson, A.J., Rochester, W., Steinberg, C.R., Roughan, M., Thompson, P., Middleton, J.F., Feng, M., Sherrington, R., Brando, V., Tilbrook, B., Ridgway, K., Allen, S., Doherty, P., Hill, K., Moltmann, T.C., 2014. IMOS national reference stations: a continental-wide physical, chemical and biological coastal observing system. PLoS One 9, e113652. https://doi.org/10.1371/journal.pone.0113652.
Macias, D., Garcia-Gorriz, E., Stips, A., 2017. Major fertilization sources and mechanisms for Mediterranean Sea coastal ecosystems. Limnol. Oceanogr. 63, 897–914. https://doi.org/10.1002/lno.10677.
Macqueen, J., 1967. Some methods for classification and analysis of multivariate observations. Proc. 5th Berkeley Symp. Mathematical Statist. Probability, pp. 281–297.
Mann, K.H., Lazier, J.R.N., 2005. Dynamics of Marine Ecosystems: Mann/Dynamics of Marine Ecosystems. Blackwell Publishing Ltd, Malden, MA USA. https://doi.org/10.1002/9781118687901.
Marchese, C., Lazzara, L., Pieri, M., Massi, L., Nuccio, C., Santini, C., Maselli, F., 2014. Analysis of chlorophyll-*a* and primary production dynamics in North Tyrrhenian and Ligurian coastal–Neritic and oceanic waters. J. Coast. Res. 690–701 https://doi.org/10.2112/JCOASTRES-D-13-00210.1.
Mattern, J.P., Dowd, M., Fennel, K., 2013. Particle filter-based data assimilation for a three-dimensional biological ocean model and satellite observations. J. Geophys. Res. Oceans 118, 2746–2760. https://doi.org/10.1002/jgrc.20213.
Mayot, N., D'Ortenzio, F., Ribera d'Alcalà, M., Lavigne, H., Claustre, H., 2016. Interannual variability of the Mediterranean trophic regimes from ocean color satellites. Biogeosciences 13, 1901–1917. https://doi.org/10.5194/bg-13-1901-2016.
Meier, H.E.M., Höglund, A., Eilola, K., Almroth-Rosell, E., 2017. Impact of accelerated future global mean sea level rise on hypoxia in the Baltic Sea. Clim. Dyn. 49, 163–172. https://doi.org/10.1007/s00382-016-3333-y.
Melaku Canu, D., Ghermandi, A., Nunes, P.A.L.D, Lazzari, P., Cossarini, G., Solidoro, C., 2015. Estimating the value of carbon sequestration ecosystem services in the Mediterranean Sea: an ecological economics approach. Glob. Environ. Change 32, 87–95. https://doi.org/10.1016/j.gloenvcha.2015.02.008.
Mélin, F., Vantrepotte, V., Clerici, M., D'Alimonte, D., Zibordi, G., Berthon, J.-F., Canuti, E., 2011. Multi-sensor satellite time series of optical properties and chlorophyll-a concentration in the Adriatic Sea. Prog. Oceanogr. 91, 229–244. https://doi.org/10.1016/j.pocean.2010.12.001.
Mozetič, P., Solidoro, C., Cossarini, G., Socal, G., Precali, R., Francé, J., Bianchi, F., Vittor, C.D., Smodlaka, N., Umani, S.F., 2010. Recent trends towards oligotrophication of the Northern Adriatic: evidence from Chlorophyll *a* Time Series. Estuar. Coasts 33, 362–375. https://doi.org/10.1007/s12237-009-9191-7.
Mozetič, P., Umani, S.F., Cataletto, B., Malej, A., 1998. Seasonal and inter-annual plankton variability in the Gulf of Trieste (northern Adriatic). ICES J. Mar. Sci. 55, 711–722. https://doi.org/10.1006/jmsc.1998.0396.
Muralikrishna, I.V., 1984. Ocean chlorophyll retrieval algorithms. Adv. Space Res. 4, 149–153. https://doi.org/10.1016/0273-1177(84)90403-4.
Nobre, A.M., Ferreira, J.G., Newton, A., Simas, T., Icely, J.D., Neves, R., 2005. Management of coastal eutrophication: Integration of field data, ecosystem-scale simulations and screening models. J. Mar. Syst. 56, 375–390. https://doi.org/10.1016/j.jmarsys.2005.03.003.
Novoa, S., Chust, G., Sagarminaga, Y., Revilla, M., Borja, A., Franco, J., 2012. Water quality assessment using satellite-derived chlorophyll-*a* within the European directives, in the southeastern Bay of Biscay. Mar. Pollut. Bull. 64, 739–750. https://doi.org/10.1016/j.marpolbul.2012.01.020.
Pastres, R., Chan, K., Solidoro, C., Dejak, C., 1999. Global sensitivity analysis of a shallow-water 3D eutrophication model. Comput. Phys. Commun. 117, 62–74. https://doi.org/10.1016/S0010-4655(98)00164-7.
Picart, S.S., Allen, J.I., Butenschön, M., Artioli, Y., Mora, L.de, Wakelin, S., Holt, J., 2015. What can ecosystem models tell us about the risk of eutrophication in the North Sea? Clim. Change 132, 111–125. https://doi.org/10.1007/s10584-014-1071-x.
Qiao, Y., Feng, J., Cui, S., Zhu, L., 2017. Long-term changes in nutrients, chlorophyll *a* and their relationships in a semi-enclosed eutrophic ecosystem, Bohai Bay, China. Mar. Pollut. Bull. 117, 222–228. https://doi.org/10.1016/j.marpolbul.2017.02.002.
Reboreda, R., Cordeiro, N.G.F., Nolasco, R., Castro, C.G., Álvarez-Salgado, X.A., Queiroga, H., Dubert, J., 2014. Modeling the seasonal and interannual variability (2001–2010) of chlorophyll-*a* in the Iberian margin. The Atlantic Iberian Margin: a research synthesis. J. Sea Res. 93, 133–149. https://doi.org/10.1016/j.seares.2014.04.003.
Ribera d'Alcalà, M., Civitarese, G., Conversano, F., Lavezza, R., 2003. Nutrient ratios and fluxes hint at overlooked processes in the Mediterranean Sea. J. Geophys. Res. Oceans 108, 8106. https://doi.org/10.1029/2002JC001650.

Rinaldi, E., Buongiorno Nardelli, B., Volpe, G., Santoleri, R., 2014. Chlorophyll distribution and variability in the Sicily Channel (Mediterranean Sea) as seen by remote sensing data. Cont. Shelf Res. 77, 61–68. https://doi.org/10.1016/j.csr.2014.01.010.

Romero, E., Peters, F., Arin, L., Guillén, J., 2014. Decreased seasonality and high variability of coastal plankton dynamics in an urban location of the NW Mediterranean. J. Sea Res. 88, 130–143. https://doi.org/10.1016/j.seares.2014.01.010.

Rydberg, L., Ærtebjerg, G., Edler, L., 2006. Fifty years of primary production measurements in the Baltic entrance region, trends and variability in relation to land-based input of nutrients. J. Sea Res. 56, 1–16. https://doi.org/10.1016/j.seares.2006.03.009.

Santoleri, R., Volpe, G., Marullo, S., Nardelli, B.B., 2008. Open Waters Optical Remote Sensing of the Mediterranean Sea, in: Remote Sensing of the European Seas. Springer, Dordrecht, pp. 103–116. https://doi.org/10.1007/978-1-4020-6772-3_8.

She, J., Allen, I., Buch, E., Crise, A., Johannessen, J.A., Le Traon, P.-Y., Lips, U., Nolan, G., Pinardi, N., Reißmann, J.H., Siddorn, J., Stanev, E., Wehde, H., 2016. Developing European operational oceanography for Blue Growth, climate change adaptation and mitigation, and ecosystem-based management. Ocean Sci. 12, 953–976. https://doi.org/10.5194/os-12-953-2016.

Shulman, I., Frolov, S., Anderson, S., Penta, B., Gould, R., Sakalaukus, P., Ladner, S., 2013. Impact of bio-optical data assimilation on short-term coupled physical, bio-optical model predictions. J. Geophys. Res. Oceans 118, 2215–2230. https://doi.org/10.1002/jgrc.20177.

Shulman, I., Gould, R.W., Frolov, S., McCarthy, S., Penta, B., Anderson, S., Sakalaukus, P., 2018. Bio-optical data assimilation with observational error covariance derived from an ensemble of satellite images. J. Geophys. Res. Oceans. 123, 1801–1813. https://doi.org/10.1002/2017JC013171.

Simon, E., Samuelsen, A., Bertino, L., Mouysset, S., 2015. Experiences in multiyear combined state-parameter estimation with an ecosystem model of the North Atlantic and Arctic Oceans using the ensemble Kalman filter. J. Mar. Syst. 152, 1–17. https://doi.org/10.1016/j.jmarsys.2015.07.004.

Simoncelli, S., Fratianni, C., Pinardi, N., Grandi, A., Drudi, M., Oddo, P., Dobricic, S., 2014. Mediterranean Sea physical reanalysis (MEDREA 1987–2015) (Version 1). https://doi.org/10.25423/medsea_reanalysis_phys_006_004.

Siokou-Frangou, I., Christaki, U., Mazzocchi, M.G., Montresor, M., Ribera d'Alcalá, M., Vaqué, D., Zingone, A., 2010. Plankton in the open Mediterranean Sea: a review. Biogeosciences 7, 1543–1586. https://doi.org/10.5194/bg-7-1543-2010.

Solidoro, C., Bastianini, M., Bandelj, V., Codermatz, R., Cossarini, G., Melaku Canu, D., Ravagnan, E., Salon, S., Trevisani, S., 2009. Current state, scales of variability, and trends of biogeochemical properties in the northern Adriatic Sea. J. Geophys. Res. Oceans 114, C07S91. https://doi.org/10.1029/2008JC004838.

Solidoro, C., Crise, A., Crispi, G., Pastres, R., 2003. An a priori approach to assimilation of ecological data in marine ecosystem models. The use of data assimilation in coupled hydrodynamic, ecological and bio-geo-chemical models of the ocean. selected papers from the 33rd International Liege Colloquium on Ocean Dynamics, held in Liege, Belgium on May 7–11th, 2001. J. Mar. Syst. 40–41, 79–97. https://doi.org/10.1016/S0924-7963(03)00014-9.

Song, H., Edwards, C.A., Moore, A.M., Fiechter, J., 2016a. Data assimilation in a coupled physical-biogeochemical model of the California current system using an incremental lognormal 4-dimensional variational approach: Part 3—Assimilation in a realistic context using satellite and in situ observations. Ocean Model. 106, 159–172. https://doi.org/10.1016/j.ocemod.2016.06.005.

Song, H., Edwards, C.A., Moore, A.M., Fiechter, J., 2016b. Data assimilation in a coupled physical-biogeochemical model of the California Current System using an incremental lognormal 4-dimensional variational approach: Part 1—Model formulation and biological data assimilation twin experiments. Ocean Model. 106, 131–145. https://doi.org/10.1016/j.ocemod.2016.04.001.

St-Laurent, P., Friedrichs, M.A.M., Najjar, R.G., Martins, D.K., Herrmann, M., Miller, S.K., Wilkin, J., 2017. Impacts of atmospheric nitrogen deposition on surface waters of the Western North Atlantic mitigated by multiple feedbacks. J. Geophys. Res. Oceans 122, 8406–8426. https://doi.org/10.1002/2017JC013072.

Storto, A., Masina, S., Dobricic, S., 2014. Estimation and impact of nonuniform horizontal correlation length scales for global ocean physical analyses. J. Atmos. Ocean. Technol. 31, 2330–2349 https://doi.org/10.1175/JTECH-D-14-00042.1.

Terauchi, G., Tsujimoto, R., Ishizaka, J., Nakata, H., 2014. Preliminary assessment of eutrophication by remotely sensed chlorophyll-*a* in Toyama Bay, the Sea of Japan. J. Oceanogr. 70, 175–184. https://doi.org/10.1007/s10872-014-0222-z.

Teruzzi, A., Cossarini, G., Lazzari, P., Salon, S., Bolzon, G., Crise, A., Solidoro, C., 2016. Mediterranean Sea biogeochemical reanalysis (CMEMS MED REA-biogeochemistry 1999–2015). https://doi.org/10.25423/MEDSEA_REANALYSIS_BIO_006_008.

Teruzzi, A., Dobricic, S., Solidoro, C., Cossarini, G., 2014. A 3-D variational assimilation scheme in coupled transport-biogeochemical models: forecast of Mediterranean biogeochemical properties. J. Geophys. Res. Oceans 119, 200–217. https://doi.org/10.1002/2013JC009277.

Testa, J.M., Li, Y., Lee, Y.J., Li, M., Brady, D.C., Di Toro, D.M., Kemp, W.M., Fitzpatrick, J.J., 2014. Quantifying the effects of nutrient loading on dissolved O_2 cycling and hypoxia in Chesapeake Bay using a coupled hydrodynamic–biogeochemical model. J. Mar. Syst. 139, 139–158. https://doi.org/10.1016/j.jmarsys.2014.05.018.

Thingstad, T.F., Rassoulzadegan, F., 1995. Nutrient limitations, microbial food webs, and biological C-pumps: suggested interactions in a P-limited Mediterranean. Mar. Ecol. Prog. Ser. 117, 299–306.

Tsiaras, K.P., Hoteit, I., Kalaroni, S., Petihakis, G., Triantafyllou, G., 2017. A hybrid ensemble-OI Kalman filter for efficient data assimilation into a 3-D biogeochemical model of the Mediterranean. Ocean Dyn. 67, 673–690. https://doi.org/10.1007/s10236-017-1050-7.

Tsiaras, K.P., Petihakis, G., Kourafalou, V.H., Triantafyllou, G., 2014. Impact of the river nutrient load variability on the North Aegean ecosystem functioning over the last decades. J. Sea Res. 86, 97–109. https://doi.org/10.1016/j.seares.2013.11.007.

Uitz, J., Stramski, D., Gentili, B., D'Ortenzio, F., Claustre, H., 2012. Estimates of phytoplankton class-specific and total primary production in the Mediterranean Sea from satellite ocean color observations. Glob. Biogeochem. Cycles 26, GB2024. https://doi.org/10.1029/2011GB004055.

Varela, M., Álvarez-Ossorio, M.T., Bode, A., Prego, R., Bernárdez, P., Garcia-Soto, C., 2010. The effects of a winter upwelling on biogeochemical and planktonic components in an area close to the Galician Upwelling Core: the sound of Corcubión (NW Spain). J. Sea Res. 64, 260–272. https://doi.org/10.1016/j.seares.2010.03.004.

Vichi, M., Lovato, T., Lazzari, P., Cossarini, G., Mlot, E.G., Mattia, G., ..., Tedesco, L., 2015. The biogeochemical flux model (BFM): equation description and user manual, BFM version 5.1. BFM Rep. Ser. 1, 104.

Vichi, M., Pinardi, N., Masina, S., 2007. A generalized model of pelagic biogeochemistry for the global ocean ecosystem. part I. Contributions from Advances in Marine Ecosystem Modelling Research, 27–29 June 2005, Plymouth, UK In: 64. pp. 89–109. https://doi.org/10.1016/j.jmarsys.2006.03.006.

Volpe, G., Colella, S., Forneris, V., Tronconi, C., Santoleri, R., 2012. The Mediterranean Ocean colour observing system – system development and product validation. Ocean Sci. 8, 869–883. https://doi.org/10.5194/os-8-869-2012.

Volpe, G., Santoleri, R., Vellucci, V., Ribera d'Alcalà, M, Marullo, S, D'Ortenzio, F, 2007. The colour of the Mediterranean Sea: global versus regional bio-optical algorithms evaluation and implication for satellite chlorophyll estimates. Remote Sens. Environ. 107, 625–638. https://doi.org/10.1016/j.rse.2006.10.017.

Yunev, O.A., Carstensen, J., Moncheva, S., Khaliulin, A., Ærtebjerg, G., Nixon, S., 2007. Nutrient and phytoplankton trends on the western Black Sea shelf in response to cultural eutrophication and climate changes. Estuar. Coast. Shelf Sci. 74, 63–76. https://doi.org/10.1016/j.ecss.2007.03.030.

Zavatarelli, M., Baretta, J.W., Baretta-Bekker, J.G., Pinardi, N., 2000. The dynamics of the Adriatic Sea ecosystem. Deep Sea Res. Part I 47, 937–970. https://doi.org/10.1016/S0967-0637(99)00086-2.

Zingone, A., Phlips, E.J., Harrison, P.J., 2010. Multiscale variability of twenty-two coastal phytoplankton time series: a global scale comparison. Estuar. Coasts 33, 224–229. https://doi.org/10.1007/s12237-009-9261-x.